RADIATION RESEARCH 161, 273–281 (2004)
0033-7587/04 $15.00

Estimating the Number of Hematopoietic or Lymphoid Stem Cells Giving Rise to Clonal Chromosome Aberrations in Blood T Lymphocytes

M. Nakano,[a,1] Y. Kodama,[a] K. Ohtaki,[a] M. Itoh,[a] A. A. Awa,[a] J. Cologne,[b] Y. Kusunoki[c] and N. Nakamura[a]

Departments of [a] Genetics, [b] Statistics and [c] Radiobiology/Molecular Epidemiology, Radiation Effects Research Foundation, 5-2 Hijiyama Park, Minami-ku, Hiroshima 732-0815, Japan

Nakano, M., Kodama, Y., Ohtaki, K., Itoh, M., Awa, A. A., Cologne, J., Kusunoki, Y. and Nakamura, N. Estimating the Number of Hematopoietic or Lymphoid Stem Cells Giving Rise to Clonal Chromosome Aberrations in Blood T Lymphocytes. *Radiat. Res.* 161, 273–281 (2004).

Quantifying the proliferative capacity of long-term hematopoietic stem cells in humans is important for bone marrow transplantation and gene therapy. Obtaining appropriate data is difficult, however, because the experimental tools are limited. We hypothesized that tracking clonal descendants originating from hematopoietic stem cells would be possible if we used clonal chromosome aberrations as unique tags of individual hematopoietic stem cells *in vivo*. Using FISH, we screened 500 blood T lymphocytes from each of 513 atomic bomb survivors and detected 96 clones composed of at least three cells with identical aberrations. The number of clones was inversely related to their population size, which we interpreted to mean that the progenitor cells were heterogeneous in the number of progeny that they could produce. The absolute number of progenitor cells contributing to the formation of the observed clones was estimated as about two in an unexposed individual. Further, scrutiny of ten clones revealed that lymphocyte clones could originate roughly equally from hematopoietic stem cells or from mature T lymphocytes, thereby suggesting that the estimated two progenitor cells are shared as one hematopoietic stem cell and one mature T cell. Our model predicts that one out of ten people bears a non-aberrant clone comprising >10% of the total lymphocytes, which indicates that clonal expansions are common and probably are not health-threatening.

INTRODUCTION

Hematopoiesis is the process by which hematopoietic stem cells differentiate into various kinds of blood cells, including lymphocytes. Long-term hematopoietic stem cells have been characterized extensively in animal model systems because they are directly relevant to hematopoietic stem cell transplantation and gene therapy (see refs. *1–3*). For example, human hematopoietic stem cells in adult bone marrow are characterized as $CD34^+$ $Thy\text{-}1^+$ Lin^- $Rh123^{dull}$ (*2*). The frequency of the long-term hematopoietic stem cells among the bone marrow cells is estimated to be 10^{-4} to 10^{-5} (*2*). Studies on the proliferation potential of hematopoietic stem cells indicate that one (or a few) long-term hematopoietic stem cell can reconstitute hematopoiesis in lethally irradiated mice (*4, 5*) and cats (*6*). In larger animals such as rhesus monkeys, single-cell engraftment studies are not possible, but it is suggested that hematopoiesis is polyclonal (*7*). Human data are rare because hematopoietic stem cell assays are limited, but in a few instances, the indication is that single hematopoietic stem cells can reconstitute nearly all of the T-lymphocyte population. For example, in a few patients suffering from hereditary severe combined immune deficiency, the affected gene reverted spontaneously to normal in apparently single committed T-cell progenitors, and the revertants proliferated so as to overcome the T-cell deficiency and greatly improve the clinical condition (*8–10*). These data demonstrate the enormous proliferation capability of single progenitor cells *in vivo* under certain conditions. It remains to be known, however, how the hematopoietic system is constructed and maintained under ordinary conditions and the number of active hematopoietic stem cells involved therein.

During the course of cytogenetic studies to evaluate the radiation dose (biodosimetry) to atomic bomb (A-bomb) survivors, we and others found identical chromosome aberrations in multiple T lymphocytes (in at least three) (*11–14*) or in both T lymphocytes and other hematopoietic cells (*14, 15*). These aberrations are termed clonal chromosome aberrations, because they are derived from single progenitor cells and produced by their large clonal expansions. The aberrations are composed mainly of translocations but occasionally include inversions as well. Clonal aberrations are observed in other radiation-exposed individuals as well (*16–22*). We considered the possibility that such clonal aberrations could serve as unique non-invasive "tags" for examining the gross clonal structure of the human hematopoietic system *in vivo*. Since 100 to 1,000 cells are usually scored for chromosome aberrations in biodosimetric studies, and the total lymphocyte number in the human body is

[1] Address for correspondence: Department of Genetics, Radiation Effects Research Foundation, 5-2 Hijiyama Park, Minami-ku, Hiroshima 732-0815, Japan; e-mail: Mimako_Nakano@rerf.or.jp.

estimated to be of the order of 10^{11} (*23*), three or more T lymphocytes with identical aberrations among the cells examined (i.e. ≥0.3% to 3% of the total T lymphocytes) give direct evidence for at least a 10^9-fold proliferation of a single progenitor cell *in vivo*. These clonal chromosome aberrations are not as specific as those seen in leukemia, and there is no evidence for their involvement in preclinical pathologies of lymphoid or myeloid malignancies. Thus they can be considered to be markers of normal proliferation of progenitor cells *in vivo*.

No systematic surveys of clonal chromosome aberrations in blood T lymphocytes have been reported. This is mainly because exposure of humans to high levels of radiation occurs only rarely, biodosimetric studies are often conducted soon after the exposure before clonally aberrant cells are generated, and these surveys are labor intensive; i.e., not only must chromosome aberrations be found, but each one must then be identified. Consequently, the mechanisms underlying the induction of clonal aberrations remain largely unknown. In the present study, using fluorescence *in situ* hybridization (FISH), we examined clonal aberrations in peripheral blood T lymphocytes from 513 A-bomb survivors. The results from 96 clones are unprecedented and provide a picture of the gross clonal structure of the T-lymphocyte pool in humans. The term "progenitor cells" as used here designates not only hematopoietic stem cells but also memory T lymphocytes because the latter also have a self-renewing function characteristic of stem cells and are able to contribute to clone formation. Therefore, understanding the structure of the hematopoietic stem cell pool from T-lymphocyte data requires knowledge of the relative contribution of hematopoietic stem cells and memory T cells to clone formation. For this purpose, we also determined the origins of ten clones.

MATERIALS AND METHODS

Blood Donors

We examined T lymphocytes in blood samples collected from 513 A-bomb survivors between 1995 and 1999. These included 91 survivors in the control group (estimated doses to bone marrow <5 mSv) and 422 exposed survivors (≥5 mSv to over 2 Sv). There were 191 males and 322 females, and the age at the time of radiation exposure varied from 0.2 to 45.9 years (mean 18.1 years). The survivors belong to the Adult Health Study (AHS) cohort of the Radiation Effects Research Foundation (RERF) in Hiroshima (*24*). The doses were estimated by the Dosimetry System 1986 (DS86; *25*). We used a fixed weighting factor of 10 for neutrons to calculate the dose equivalent in sieverts (*26*).

The study was approved by the RERF Human Investigation Committee.

Cell Culture

Two milliliters of heparinized whole blood from each donor was cultured for 48 h in upright 25-cm² tissue culture flasks (Corning, Funabashi) in 10 ml RPMI 1640 medium (Sigma-Aldrich, Tokyo) supplemented with glutamine (Nissui, Tokyo), 20% fetal calf serum (Gibco-BRL, Tokyo), and phytohemaggulutinin (PHA, 0.15 mg/ml, Murex Biotech, Tokyo). Colchicine (0.15 μg/ml, Wako, Osaka) was added during the last 2 h, and metaphase spreads were prepared as described previously (*27*).

FISH and Q-Banding

Five hundred metaphases per blood sample were examined with FISH painting of chromosomes 1, 2 and 4 (*13*). The *x* and *y* coordinates of all aberrant cells bearing at least one exchange between the painted and unpainted chromosomes were recorded for subsequent Q-banding analyses (*28*) done on the same metaphases to identify the unpainted counterpart chromosomes and to localize the approximate breakpoints involved in each translocation. Identification of the painted chromosomes involved could be achieved easily in most of the cases. In about one-third of the suspected clonal cases, when Q-band information failed to identify the unpainted counterpart chromosome, additional FISH was carried out using probes specific for the suspected chromosomes (Cambio, Cambridge, UK). Each set of probes was labeled with a different color. In our FISH analysis, the painted chromosomes (chromosomes 1, 2 and 4) comprise about 22% of the genome, so that the observed frequency (F_P) of translocations between painted and unpainted chromosomes represents about 1 in 2.8 (36%) of the total translocations among the whole set of 46 chromosomes, denoted as the genome-equivalent translocation frequency, F_G. The factor 2.8 is derived in ref. (*13*). Whenever clonal aberrations were observed, they were counted as single events to calculate F_P. Complex translocations (Cx) or insertions were occasionally observed (about 5% of the total stable, exchange-type aberrations) and were included when calculating F_P. They were regarded as equivalent to either single translocations (Cx with one or two color changes or any insertion) or two translocations (Cx with three or four color changes). A few clones were composed of Cx or insertions (see our website for the details: http://www.rerf.jp/eigo/scidata/cl2003.htm).

Definition of Clonal Aberrations

We based our final judgment of whether an aberration was clonal on the locations of the breakpoints (chromosome arms and approximate length of the exchanged segments) involved in every translocation. The minimum number of cells accepted as being clonal was set as three to avoid an *in vitro* artifact resulting from some cells entering a second mitosis during the 48-h culture period. The smallest detectable population size (clone fraction, C_F) was therefore 0.6%, i.e. three per 500 cells examined.

Determination of Clonal Origins

Blood lymphocytes from five survivors who had previously been identified as clone carriers (*11*) were examined in detail to determine whether the clones originated from hematopoietic stem cells or mature T cells. The lymphocytes were first labeled with mouse anti-human CD4 or CD8 antibody that was conjugated with microbeads (Miltenyi, Sunnyvale, CA), and $CD4^-$ or $CD8^-$ fractions were collected by passing the cells through a magnetic column apparatus (Miltenyi, Bergisch Gladbach, Germany) (*29*). Subsequently, the cells were labeled with mouse anti-human CD45RA antibody (DAKO, Glostrup, Denmark) followed by goat anti-mouse IgG antibody that was conjugated with microbeads and were subjected to magnetic sorting to obtain both the $CD45RA^-$ and $CD45RA^+$ fractions. Four cell fractions were thus obtained for each blood sample: $CD45RA^+CD8^-$ (we considered them as naïve $CD4^+$ T cells, abbreviated as CD4Tn), $CD45RA^-CD8^-$ (memory $CD4^+$ T cells, CD4Tm), $CD45RA^+CD4^-$ (naïve or effector $CD8^+$ T cells, CD8TnTe; ref. *30*), and $CD45RA^-CD4^-$ (memory $CD8^+$ T cells, CD8Tm; ref. *30*). The major portions of the sorted cell populations were cultured *in vitro* for FISH analysis using whole chromosome painting probes (Vysis, Downers Grove, IL) selected for each clone and labeled with different fluorescent dyes. At the same time, small portions of the cell populations were used for assessment of the frequency of contaminating T cells from other subsets by flow cytometry (FACScan, Becton-Dickinson, San Jose, CA). In

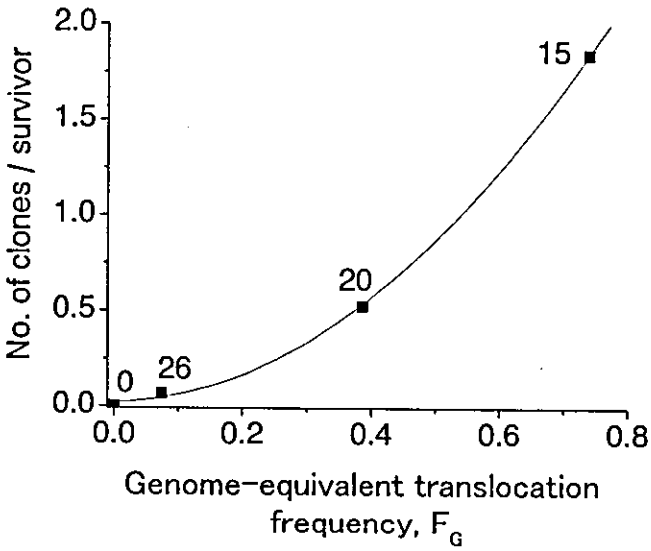

FIG. 1. The number of clones observed per survivor in relation to the genome-equivalent translocation frequency, F_G. Number of cases is shown above each symbol.

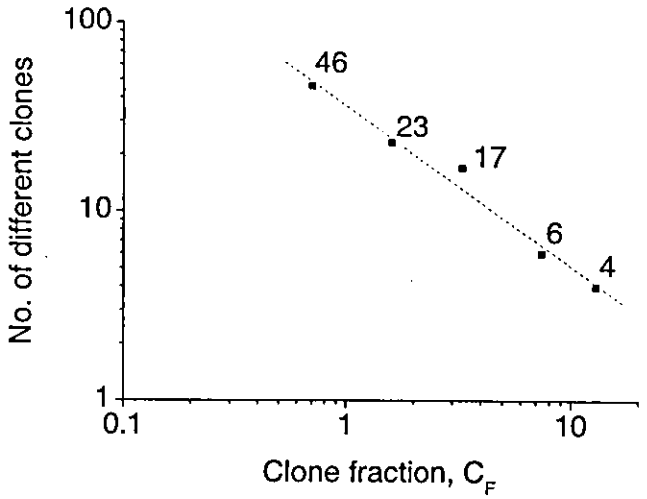

FIG. 2. Grouped number of clones in relation to the fraction of clonal cells (C_F) among the 500 T lymphocytes scored. Number of cases is shown above each symbol.

brief, we found that CD4$^+$ cells contaminated 4 ± 3% (range from 1% to 8%) of the CD8TnTe fractions and 1.0 ± 0.9% (range from 0% to 2%) of the CD8Tm fractions. Likewise, CD8$^+$ cells contaminated 10 ± 7% (range from 3% to 21%) of the CD4Tn fractions and 0.10 ± 0.07% (range from 0% to 0.2%) of the CD4Tm fractions.

Theoretical Distribution of Clone Size

Suppose that the total lymphocyte pool comprises n lineages (or clonal populations) labeled as $i = 1, 2, 3, \ldots, n$, and each lineage occupies a proportion (p_i) of the lymphocytes ($\Sigma p_i = 1$). The simplest model assumes that each lineage has exactly the same p_i, so that $p_i = 1/n$. Even under such conditions, however, the observed clone sizes are not the same but vary due to sampling fluctuation since we scored only 500 cells. The probability of detecting k clonal cells for a given lineage i among 500 cells examined is described by a binomial function as

$$\Pr_i(k) = \left[\frac{500!}{k!(500-k)!}\right] p_i^k (1-p_i)^{500-k}. \quad (1)$$

To allow the equation to be applicable to more general conditions where p_i varies following a certain distribution, we do not know which lineage the observed clone came from (e.g., whether the observed clone i came from a large lineage or a small one). Then the equation is rewritten by adding a multiplier $f(p_i)$ which represents the chance that the observed clone came from the clone with proportion p_i:

$$\Pr(k) = \sum_i f(p_i)\left[\frac{500!}{k!(500-k)!}\right] p_i^k (1-p_i)^{500-k}, \quad (2)$$

where $f(p_i)$ is the probability density (distribution) of p_i. This equation is the overall (marginal) probability of observing a clone with k cells per 500. This marginal probability is the weighted sum of the above binomial probabilities, where the sum is taken over all lineages i weighted by the probability distribution of the proportions p_i.

One model for $f(p_i)$ that we thought was more realistic than the equal-size model was to assume that the p_i's were equal on average but that there was random variation in individual p_i values. This was modeled by defining $f(p_i)$ to be centered at $1/n$ with some dispersion (we did not distinguish between intra- and interindividual variation). Other models for $f(p_i)$, such as the beta and exponential distributions, were also evaluated.

The expected number of clones for each size k between 3 and the maximum observed size of 89 (17.8%) was computed by simulation, generating random values of the proportions p_i according to the hypothesized model and calculating the marginal probabilities $\Pr(k)$.

RESULTS

Clone Detection is Affected by the Individual Translocation Frequency and the Clonal Population Size

After examination of 500 T lymphocytes from each of these 513 survivors, we identified 96 different clones carried by 61 individuals. (Detailed information on the clones is presented on our website: http://www.rerf.jp/eigo/scidata/cl2003.htm.) We found that the probability of finding a clone per individual increased more than linearly with F_G as shown in Fig. 1 (F_G is the estimated translocation frequency in the whole genome, which is 2.8 times the observed translocation frequency, F_P, with our FISH; see the Materials and Methods). Fitting the data with the linear-quadratic equation gave $y = 0.02 + 0.10F_G + 3.2F_G^2$.

The observed clones varied extensively in the number of clonal cells per 500 cells examined; namely, 46 were small clones comprising less than 6 cells per 500 cells ($C_F <$ 1.2%). A few clones had $C_F > 5\%$; six had C_F of 5–10%, and in four clones the C_F was ≥10%. The largest clone comprised about 18% (89 cells/500). Plotting the log of the number of different clones as a function of the log of C_F gave a straight line with a negative slope (Fig. 2). In this figure, we grouped C_F on the log (base 2) scale so that the points could distribute with roughly equal intervals on the x axis, i.e. C_F of 0.6% (minimum size)–1.2%, 1.2–2.4%, 2.4–4.8%, etc. Linear regression analysis produced the fitted equation: log (number of clones) = $1.56 - 0.85 \times \log C_F$. In other words, for every doubling of the mean C_F, the number of clonal events decreased by roughly about half.

We found no association between the clone size, C_F, and

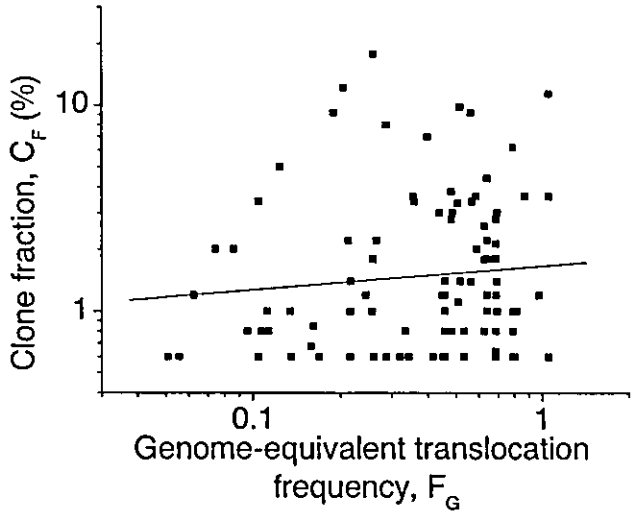

FIG. 3. Distribution of clonal cell fraction, C_F, in relation to individual frequency of translocations expressed as genome-equivalent frequency, F_G.

individual frequencies of translocations with FISH (P = 0.38), as shown in Fig. 3. In other words, large (or small) clones are not related to exposure to higher (or lower) doses of radiation.

Development of a Model

While attempting to model the gross clonal structure of the lymphocyte pool, we first suspected that the actual population sizes of clones *in vivo* might have been more or less equal on average but the frequency of clones observed apparently decreased with an increase in C_F due to sampling fluctuations produced by a common binomial distribution. Imagine one large blood sample that contains lymphocytes with identical aberrations at a true frequency of a/500, and prepare multiple slides from the sample and score 500 cells on each slide. Then the probability of observing the clonal cells k times out of 500 cells (C_F = k/500) would follow a binomial function (an upward convex distribution) and the probability gives the highest value at k = a and declines as k increases beyond a, which might explain the results in Fig. 2.

We examined the simplest model that all lineages comprising the total lymphocyte pool are exactly equal in size; i.e., the proportion of a lineage p_i = 1/n (Eq. 1). The results after computer simulations on the relationship between the expected number of clones observed and the C_F are shown in Fig. 4A (left) along with the hypothetical distribution of the p_i (right), which is a single mass at 1/n. The model obviously did not fit the observed C_F distribution because the binomial probabilities decreased too quickly to accommodate the large clones observed. The fit was worse with the larger value of n, because the larger n is, the smaller the p_i's, and hence the chance of observing a large clone is smaller (results for n = 100 and 1,000 are shown in Fig.

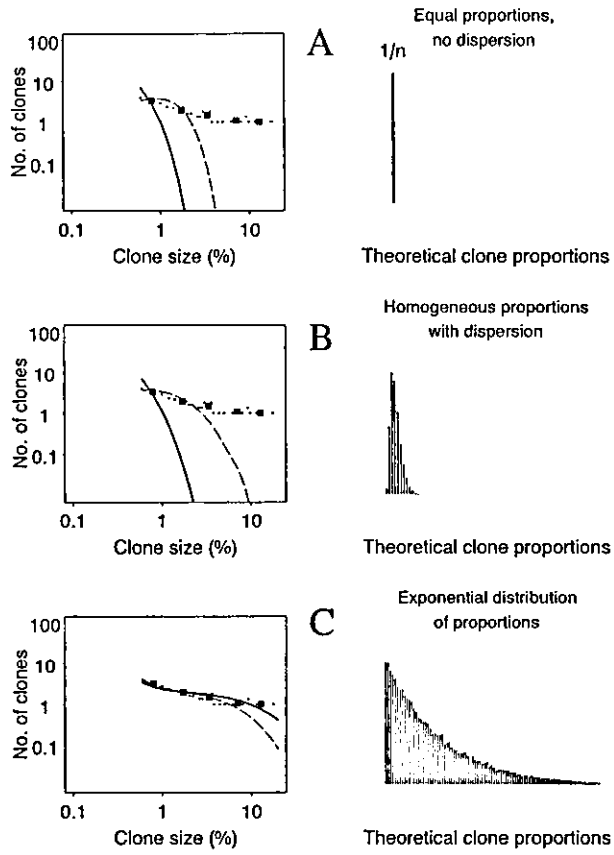

FIG. 4. Results of computer simulations on the number of clones expected under different hypothetical distributions of clone sizes (proportions p_i). Panel A: All p_i's are equal. Panel B: p_i's are equal on average, but with dispersion (logit normally distributed). Panel C: Exponential distribution of p_i. Right side: Hypothesized distribution of p_i. Left side: Observed data (points) and fitted values (lines) according to binomial sampling of 500 cells. The mean numbers of clones for grouped points corresponding to the groups of Fig. 2 are also shown (■). The solid line is the fit assuming n = 1,000 lineages; the dashed line is for n = 100.

4). (Note that the simulations used individual data so that the grouped numbers of clones shown here are the means of more restricted, individual units of C_F and hence differ from the numbers in Fig. 2.)

One modified model that introduced a variance of 0.2 in the distribution function $f(p_i)$ which is normal in the logit of p (logit $\{p\}$ = ln $\{p[1 - p]\}$) in Eq. (2) gave the fit shown in Fig. 4B. This model produced slightly more clones of larger sizes relative to the results with equal p_i, but it still did not fit the data despite a fairly large amount of dispersion in the p_i. We also examined other values of the variance and other types of models for the dispersion in the p_i, but models that had a modal value greater than 0 generally failed to fit the observed data over most of the range (results not shown). The results strongly indicate that the observed inverse relationship between the number of clones observed and the C_F (Fig. 2) cannot be explained by assuming homogeneous distribution in the p_i and sam-

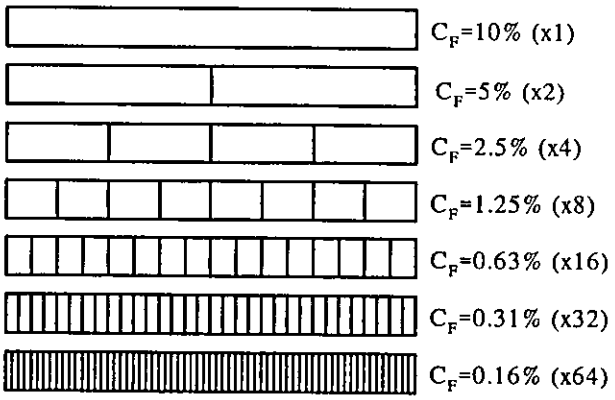

FIG. 5. Variable-size clone model of the lymphocyte pool. The open rectangles of various sizes represent clonal lymphocyte populations that were invariably derived from single progenitor cells. Numbers in parentheses indicate the relative frequency of progenitor cells (or their lineages) across the groups of clones in the same size range in relation to the mean C_F. Clones larger than 10% or smaller than 0.16% are not shown.

pling fluctuation, which leads us to consider a heterogeneous distribution.

In characterizing the heterogeneity, we thought that the hypothetical model stipulated that the probability of observing a clone should decrease by a factor of 2 as the clone size was doubled as seen in Fig. 2, namely, an exponential distribution model for the p_i. The results of the simulations based on assuming the exponential distribution are shown in Fig. 4C. Here the mean of the exponential distribution was chosen so as to minimize the binomial weighted sum of squared deviations between observed points and fitted line in the left side of the figure. Models with n = 100 and 1,000 both fit the data much better than the two previous models, but the exponential model with n = 1,000 fit the largest clones better than that with n = 100.

Figure 5 is a schematic representation of the exponential model. Although theoretically the C_F may take any value from 3 to 500 per 500 (i.e., C_F values vary continuously), for the sake of simplicity we grouped the C_F on the log (base 2) scale as plotted in Fig. 2. The rectangles of various sizes represent clonal lymphocyte populations of various sizes but were invariably derived from single progenitor cells that gave rise to various numbers of progeny.

After modeling the relative frequency of progenitor cells that might give rise to progeny of various numbers, we were able to estimate the absolute number of progenitor cells (N) that can produce clonal populations of detectable sizes (i.e. $C_F \geq 0.6\%$) in an individual. This was achieved by estimating N at different levels of F_P obtained by solving the equation

$$\text{Number of clonal events observed} = N \times \text{number of survivors} \times \text{mean } F_P.$$

The result was that N increased with F_P (Table 1). Linear regression analysis gave the relationship N = 1.8 (±0.7) + 18 (±4) × F_P. In other words, the estimated N was about two (one to three) at the lowest F_P and increased to about seven at the highest F_P.

Possible Effect of Age at the Time of Radiation Exposure

We wanted to know whether the clone formation is affected by the age at the time of radiation exposure. For this purpose, we calculated the expected number of clones for each individual based on the results shown in Fig. 1. Subsequently, the survivors were grouped according to the age at the time of radiation exposure, and the ratio of the number of observed clones to the number of expected clones was obtained. The results are shown in Fig. 6. Although the trend in the linear regression gave a positive slope, it was nonsignificant (P = 0.35).

Relative Contribution of Hematopoietic Stem Cells and Mature T Cells to Clone Formation

The number of progenitor cells estimated above includes both hematopoietic stem cells and mature T lymphocytes. To assess the absolute numbers of hematopoietic stem cells and mature T cells involved in clone formation, we determined the origin of ten clones. The results are summarized in Table 2. Among these, four clones, A1, B1, C and D, were assigned as originating from hematopoietic

TABLE 1
Number of Clones Observed and Estimated Number of Progenitor Cells per Survivor at Different Levels of Translocation Frequency Detected with FISH

F_P (mean)	No. of survivors	No. of clones	No. of survivors with clonal aberrations	No. of clones/survivor	No. of progenitor cells/survivor[a] (N)
0 (0)	6	0	0	0	1.84[b]
$0 < F_P \leq 0.1$ (0.026)	427	29	26	0.068	2.61
$0.1 < F_P \leq 0.2$ (0.138)	61	32	20	0.524	3.80
$F_P > 0.2$ (0.265)	19	35	15	1.84	6.95
Total (0.048)	513	96	61		

[a] The number of progenitor cells that could give rise to clonal descendants comprising ≥0.6% of the lymphocyte pool.

[b] Number (1.84) was estimated from the y axis intercept after the linear regression of the data, namely N = 1.8 (±0.7) + 18 (±4) × F_P.

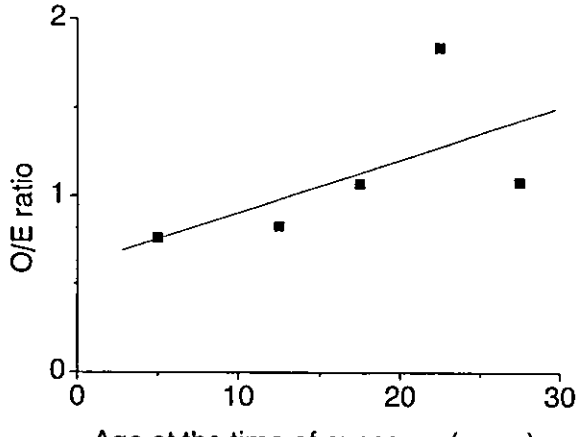

FIG. 6. Ratio of observed to expected numbers of clonal aberrations in relation to age at the time of radiation exposure.

stem cells since identical translocations were clearly observed in both the $CD8^-$ and $CD4^-$ T-cell fractions (we considered them as $CD4^+$ and $CD8^+$ T cells, respectively). Two clones, B2 and E1, were assigned as probably being derived from hematopoietic stem cells. This is because whereas only four clonal cells each were observed in $CD4^-$ (clone B2) or $CD8^-$ (clone E1) cell fractions, these clonal cells could not be explained by the frequency of contaminating cells assessed by flow cytometry. For instance, for clone B2, $CD8^-$ cells were found to contaminate only 0.9% of the CD8TnTe fraction and 0% of the CD8Tm fraction. As for clone E1, the one clonal cell found in the CD4Tn fraction could be explained as coming from the 14% contaminating $CD4^-$ cells (the expected number is $0.14 \times 12 = 1.7$), whereas the three clonal cells in the CD4Tm fraction could not be attributed to contaminating cells because there were only 0.1% contaminating $CD4^-$ cells. The remaining four clones were assigned as originating from mature T cells, either single $CD4^+$ T cells (A2 and E2) or $CD8^+$ T cells (A3 and B3). Clone A2 consisted of six clonal cells that were found only in the CD4Tm fraction. Clone E2 was also considered to come from the CD4Tm fraction because, although four clonal cells were found in the CD4Tn fraction, the fraction contained 16% contaminating CD4Tm cells, which could account for 3.8 clonal cells (0.16×24). Clones A3 and B3 were represented by clonal cells mostly in the $CD8^+$ fraction. One clonal cell in the CD4Tm fraction of clone B3 was regarded as probably due to contamination of $CD8^+$ cells. Overall, about half of the ten clones examined (i.e. at least four clones and probably an additional two) originated from hematopoietic stem cells. Since at least five of these hematopoietic stem cell-derived clones still involve CD4Tn cells 50 years after the exposure to radiation, they appear to have originated from long-term hematopoietic stem cells rather than from committed lymphoid progenitor cells, which should have a limited life span.

In summary, the results indicate that our estimation of about two progenitor cells capable of forming T-lymphocyte clones in an unexposed individual would be shared roughly by the long-term hematopoietic stem cells and memory T-lymphocyte population, i.e. one cell of each cell type.

TABLE 2
Summary for the Origins of Ten Clones

Clone name	Clonal translocation	Fraction of clonal cells in various subpopulations: Total T cells	$CD8^-$: CD4Tn	$CD8^-$: CD4Tm	$CD4^-$: CD8TnTe	$CD4^-$: CD8Tm	Assigned origin
A1	t(2;12)	35/500 (7%)	24/500 (5%)	25/500 (5%)	51/500 (10%)	13/243 (5%)	Hematopoietic stem cell
B1	t(1;8)	14/492 (3%)	17/500 (3%)	3/500 (0.6%)	7/500 (1%)	0/249 (0%)	Hematopoietic stem cell
C	t(4;6) t(5;13)	39/500 (8%)	49/500 (10%)	4/500 (0.8%)	61/495 (12%)	Not done	Hematopoietic stem cell
D	t(2;4)	137/300 (46%)	128/300 (43%)	68/300 (23%)	135/300 (45%)	Not done	Hematopoietic stem cell
B2	t(1;21) t(11;16) t(18;20)	8/492 (2%)	8/500 (2%)	1/500 (0.2%)	2/500 (0.4%)	2/249 (0.8%)	Hematopoietic stem cell
E1	t(3;4)	2/500 (0.4%)	1/500 (0.2%)	3/500 (0.6%)	12/500 (2%)	31/500 (6%)	Hematopoietic stem cell
A2	t(1;12) t(2;B)	0/500 (0%)	0/500 (0%)	6/500 (1%)	0/500 (0%)	0/243 (0%)	$CD4^+$
E2	t(2;2)	4/500 (0.8%)	4/500 (0.8%)	24/500 (5%)	1/500 (0.2%)	0/500 (0%)	$CD4^+$
A3	t(2;14)	4/500 (0.8%)	0/500 (0%)	0/500 (0%)	24/500 (5%)	31/243 (13%)	$CD8^+$
B3	t(1;Y)	0/492 (0%)	0/500 (0%)	1/500 (0.2%)	6/500 (1%)	5/249 (2%)	$CD8^+$

Notes. Blood T cells were fractionated using anti-CD4, anti-CD8, and anti-CD45RA antibodies to obtain four fractions: $CD8^-$ or $CD4^-$, and $CD45RA^+$ or $CD45RA^-$ fractions. Cells in $CD8^-$ or $CD4^-$ fractions were regarded as $CD4^+$ or $CD8^+$, respectively. Subsequently, the frequency of cells bearing the clonal aberrations was determined with FISH using a combination of chromosome-specific probes selected for each clone. The frequency of clonal aberrations in the whole T-cell population is also shown. Clone name: (A to E) Letter denotes donor code and numbers 1 to 3 denote different clones carried by the same donor. CD4Tn and CD4Tm are naïve and memory $CD4^+$ T cells, and CD8TnTe and CD8Tm stand for naïve or effector $CD8^+$ and memory $CD8^+$ T cells, respectively.

DISCUSSION

Validation of the Model

We tested whether our model was consistent with other clonal aberration data. We found four data sets for radiation-exposed subjects that were eligible for testing the hypothesis. The full descriptions of the cases will be published elsewhere (*31*), but the result is that the predicted number of clones based on our model agrees with the observed number of cases; the total numbers were 40 observed compared to 35.9 calculated.

For example, Awa (*11*) used a conventional solid Giemsa staining method (not G-banding method) to score 100 T cells per blood sample (detectable clone size is 3 or more cells per 100 cells; $C_F \geq 3\%$) and found 7 clones among 71 A-bomb survivors whose mean translocation frequency was 0.14 (*27*). Since the observed mean translocation frequency was 0.14, the true mean frequency was likely to have been 0.14/0.7 = 0.20 because the translocation frequency detected by the cytogenetic method used is about 30% lower than the estimated genome-equivalent translocation frequency, F_G, with our FISH (*32*). This corresponds to $F_P = 0.20/2.8 = 0.071$ by our FISH method because it detects about 1 in 2.8 of the total translocations in the whole set of 46 chromosomes (*13*). At this level of F_P, the estimated number of N that can form clones of 3% or larger in an individual is estimated from the linear regression of the data in Table 1; namely, $N = (1.8 + 18 \times 0.071) \times (100/500) = 0.62$. The term (100/500) corrects for the difference in minimum C_F detectable by Giemsa staining (3% after scoring 100 cells) compared to FISH (0.6% after scoring 500 cells) analysis (*31*). Thus the expected number of clones making up ≥3% of total cells as detected by the conventional method is 71 (survivors) × 0.14 (mean translocation frequency observed) × 0.62 (N) = 6.2, which is close to the observed number of 7.

No Evidence that Clonal Cells are Abnormal

Generalization of the present model requires exclusion of the possibility that clonal expansions are the result of preclinical pathologies of hematological disorders. Several observations indicate that this possibility is low, specifically: (1) Among the six chromosome arms painted with FISH, translocation breakpoints of the clones did not indicate any skewed distributions but were in proportion to the DNA content ($\chi^2 = 4.39$, $P = 0.5$ at $\varphi = 5$). This finding agrees with observations that interchromosomal exchanges occur mostly at random among chromosomes (i.e. in proportion to the DNA content) after radiation exposure (*13, 33*). (2) In A-bomb survivors, the risk of lymphoma never increased; most of the excess risk of leukemia occurred in the first 15 years after exposure, and the leukemia risk is currently close to the control level (*26*). (3) T lymphocytes comprising one large clone ($C_F = 8\%$), confirmed as having originated from a single hematopoietic stem cell, were functionally heterogeneous and mature (*14*). (4) In a few survivors, population sizes of several large clones ($C_F \geq 3\%$) remained roughly constant for nearly 20 years (Awa, unpublished observation). Therefore, we are inclined to believe that the process of forming large clonal T-cell populations is not caused primarily by a growth advantage conferred by a specific chromosome change in progenitor cells carrying the aberrations but probably by a random-hit event. This notion is in line with the finding that the numbers of clones observed under different conditions are predictable by a simple equation (previous section).

T-Lymphocyte Clones Exist among Normal Cells

If we accept that radiation exposure branded a fraction of the progenitor cell population randomly with different chromosome aberrations so that the clonally related progeny become detectable, a logical consequence is that many other clones (originated from either hematopoietic stem cells or memory T cells), which go undetected, exist among normal T lymphocytes. This notion is supported by two findings. (1) At $F_P = 0$, N is not zero but is about 2 (1 to 3) (Table 1). (2) C_F was not related to F_G (Fig. 3). In other words, clonal chromosome aberrations are rarely found, whereas clonally derived T lymphocytes are commonly present. Indeed, clonal expansion of mature but non-aberrant T lymphocytes is reported for $CD8^+$ or $CD4^-CD8^-$ T cells using identical T-cell receptor gene rearrangement patterns as markers (*34–40*). The clones may constitute 10% or more of the blood T lymphocytes (*38–40*). One implication in biodosimetry is that although it is widely recognized that finding clonal aberrations and counting them as single events is critically important to avoid overestimation of the dose, we can never detect clonal populations among normal cells. However, whereas the clones of normal karyotype inflate the denominator for calculating the translocation frequency, clonal aberrations affect the numerator. Therefore, normal clones have less of an effect on biodosimetry than aberrant clones. For example, if there existed one normal clone comprising 5% of the total T lymphocytes (this seems to occur commonly; see below), the observed translocation frequency may be overestimated by only about 5%, which is acceptably small.

Large Clonal Expansion itself Probably is not Detrimental

Our model allows us to estimate the number of progenitor cells that contribute significantly to the total pool of T lymphocytes through formation of large clonal populations. Since the frequency of progenitor cells was estimated as being inversely proportional to C_F (Fig. 2) and N as being about two in forming clonal populations comprising ≥0.6% of the total T lymphocytes in unexposed people, we envisage that one-half of N (i.e. 2/2 = 1 cell) would produce a clone with $C_F = 0.6$–1.2%, one-fourth (2/4 = 0.5 cells) a clone with $C_F = 1.2$–2.4% (i.e. two times 0.6–1.2%), ... 1/16 (2/16 = 0.13 cells) a clone with $C_F = 4.8$–9.6%,

1/32 (2/32 = 0.06 cells) a clone with C_F = 9.6–19%, 1/64 (2/64 = 0.03 cells) a clone with C_F = 19–38%, etc. Therefore, the number of progenitor cells capable of forming clones comprising ≥10% or 5%, for example, of the total T lymphocytes in an ordinary individual is estimated as about 0.11 (i.e. 0.06 + 0.03 + 0.015) or 0.24 (i.e. 0.13 + 0.11), respectively. In other words, one individual out of about 10 or 4 bears one T-lymphocyte clone comprising ≥10% or 5% of the total T lymphocytes, originating from a single hematopoietic stem cell or mature T cell (but such clones remain invisible because they do not carry chromosomal tags). This means that huge clonal expansion of a few long-term hematopoietic stem cells or mature T lymphocytes by 10^9- to 10^{10}-fold is commonly taking place among ordinary individuals. Therefore, apart from uncontrolled proliferation of T lymphocytes observed recently in two patients who had undergone gene therapy for immune deficiency[2] (*42*), extensive proliferation of hematopoietic stem cells or even mature T lymphocytes probably is not health-threatening.

ACKNOWLEDGMENTS

We thank Drs. S. Wolff and C. A. Waldren for reading the manuscript, Dr. S. Kyoizumi for helping us in flow cytometric analysis of contaminating subsets, Drs. D. Pierce and S. Abrahamson for their valuable comments, Dr. D. J. Pawel for statistical help, and the Cytogenetics laboratory staff for technical assistance. The Radiation Effects Research Foundation (RERF), Hiroshima and Nagasaki, Japan is a private, non-profit foundation funded equally by the Japanese Ministry of Health, Labour and Welfare (MHLW) and the U.S. Department of Energy (DOE), the latter through the National Academy of Sciences. This publication was supported by RERF Research Protocol RP8-93.

Received: May 20, 2003; accepted: October 31, 2003

REFERENCES

1. H. L. Aguila, K. Akashi, J. Domen, K. L. Gandy, E. Lagasse, R. E. Mebius, S. J. Morrison, J. Shizuru, S. Strober and I. L. Weissman, From stem cells to lymphocytes: Biology and transplantation. *Immunol. Rev.* **157**, 13–40 (1997).
2. S. J. Morrison, N. Uchida and I. L. Weissman, The biology of hematopoietic stem cells. *Annu. Rev. Cell Dev. Biol.* **11**, 35–71 (1995).
3. N. B. Ivanova, J. T. Dimos, C. Schaniel, J. A. Hackney, K. A. Moore and I. R. Lemischka, A stem cell molecular signature. *Science* **298**, 601–604 (2002).
4. C. T. Jordan and I. R. Lemischka, Clonal and systemic analysis of long-term hematopoiesis in the mouse. *Genes Dev.* **4**, 220–232 (1990).
5. M. Osawa, K. Hanada, H. Hamada and H. Nakauchi, Long-term lymphohematopoietic reconstitution by a single CD34-low/negative hematopoietic stem cell. *Science* **273**, 242–245 (1996).
6. J. L. Abkowitz, M. T. Persik, G. H. Shelton, R. L. Ott, J. V. Kiklevich, S. N. Catlin and P. Guttorp, Behavior of hematopoietic stem cells in a large animal. *Proc. Natl. Acad. Sci. USA* **92**, 2031–2035 (1995).
7. H. J. Kim, J. F. Tisdale, T. Wu, M. Takatoku, S. E. Sellers, P. Zickler, M. E. Metzger, B. A. Agricola, J. D. Malley and C. E. Dunbar, Many multipotential gene-marked progenitor or stem cell clones contribute to hematopoiesis in nonhuman primates. *Blood* **96**, 1–8 (2000).

[2] http://www.ap-hp.fr/actualite/2-cp-us.htm.

8. T. Wada, S. H. Schurman, M. Otsu, E. K. Garabedian, H. D. Ochs, D. L. Nelson and F. Candotti, Somatic mosaicism in Wiskott-Aldrich syndrome suggests *in vivo* reversion by a DNA slippage mechanism. *Proc. Natl. Acad. Sci. USA* **98**, 8697–8702 (2001).
9. R. Hirschhorn, D. R. Yang, J. M. Puck, M. L. Huie, C. K. Jiang and L. E. Kurlandsky, Spontaneous *in vivo* reversion to normal of an inherited mutation in a patient with adenosine deaminase deficiency. *Nat. Genet.* **13**, 290–295 (2001).
10. P. Bousso, V. Wahn, I. Douagi, G. Horneff, C. Pannetier, F. Le Deist, F. Zepp, T. Niehues, P. Kourilsky and G. de Saint Basile, Diversity, functionality, and stability of the T cell repertoire derived *in vivo* from a single human T cell precursor. *Proc. Natl. Acad. Sci. USA* **97**, 274–278 (2002).
11. A. A. Awa, Cytogenetic and oncogenic effects of the ionizing radiations of the atomic bomb, In *Chromosomes and Cancer* (J. L. German, Ed.), pp. 637–674. Wiley, New York, 1974.
12. A. A. Awa, Chromosomal aberrations in atomic bomb survivors. *Gann Monogr. Cancer Res.* **35**, 175–189 (1988).
13. J. N. Lucas, A. A. Awa, T. Straume, M. Poggensee, Y. Kodama, M. Nakano, K. Ohtaki, H-U. Weier, D. Pinkel and G. Littlefield, Rapid translocation frequency analysis in humans decades after exposure to ionizing radiation. *Int. J. Radiat. Biol.* **62**, 53–63 (1992).
14. Y. Kusunoki, Y. Kodama, Y. Hirai, S. Kyoizumi, N. Nakamura and M. Akiyama, Cytogenetic and immunologic identification of clonal expansion of stem cells into T and B lymphocytes in one atomic-bomb survivor. *Blood* **86**, 2106–2112 (1995).
15. T. Amenomori, T. Honda, M. Otake, M. Tomonaga and M. Ichimaru, Growth and differentiation of circulating hemopoietic stem cells with atomic bomb irradiation-induced chromosome abnormalities. *Exp. Hematol.* **16**, 849–854 (1988).
16. K. E. Buckton, A. O. Langlands and G. E. Woodcock, Cytogenetic changes following Thorotrast administration. *Int. J. Radiat. Biol.* **12**, 565–577 (1967).
17. T. Ishihara, S. Kohno, I. Hayata and T. Kumatori, A nine-year cytogenetic follow-up of a patient injected with Thorotrast. *Hum. Genet.* **42**, 99–108 (1978).
18. K. Salassidis, E. Schmid, R. U. Peter, H. Braselman and M. Bauchinger, Dicentric and translocation analysis for retrospective dose estimation in humans exposed to ionizing radiation during the Chernobyl nuclear power plant accident. *Mutat. Res.* **311**, 39–48 (1994).
19. K. Salassidis, V. Georgiadou-Schmacher, H. Braselmann, P. Muller, R. U. Peter and M. Bauchinger, Chromosome painting in highly irradiated Chernobyl victims: A follow-up study to evaluate the stability of symmetrical translocations and the influence of clonal aberrations for retrospective dose estimation. *Int. J. Radiat. Biol.* **68**, 257–262 (1995).
20. H. Zitzelsberger, H. Hessel, K. Salassidis, H. Mittermuller and M. Bauchinger, Molecular genetic characterization of the Philadelphia chromosome detected in reactor personnel highly exposed to radiation from the Chernobyl accident. *Cancer Genet. Cytogenet.* **104**, 86–93 (1998).
21. K. L. Johnson, J. Nath, J. M. Pluth and J. D. Tucker, The distribution of chromosome damage, non-reciprocal translocations and clonal aberrations in lymphocytes from Chernobyl clean-up workers. *Mutat. Res.* **439**, 77–85 (1999).
22. A. T. Natarajan, R. C. Vyas, J. Weigant and M. P. Curado, A cytogenetic follow-up study of the victims of a radiation accident in Goiania (Brazil). *Mutat. Res.* **247**, 103–111 (1991).
23. F. Trepel, Number and distribution of lymphocytes in man. A critical analysis. *Klin Wochenschr.* **52**, 511–515 (1974).
24. M. Yamada, H. Sasaki, F. Kasagi, M. Akahoshi, Y. Mimori, K. Kodama and S. Fujiwara, Study of cognitive function among the Adult Health Study (AHS) population in Hiroshima and Nagasaki. *Radiat. Res.* **158**, 236–240 (2002).
25. W. C. Roesch, Ed., *Final Report on US-Japan Joint Reassessment of Atomic Bomb Radiation Dosimetry in Hiroshima and Nagasaki.* Radiation Effects Research Foundation, Hiroshima, 1987.
26. D. A. Pierce, Y. Shimizu, D. L. Preston, M. Vaeth and K. Mabuchi,

Studies of the mortality of atomic bomb survivors. Report 12, Part I. Cancer: 1950–1990. *Radiat. Res.* **146**, 1–27 (1996).

27. A. A. Awa, T. Sofuni, T. Honda, M. Itoh, S. Neriishi and M. Ohtake, Relationship between the radiation dose and chromosome aberrations in atomic bomb survivors of Hiroshima and Nagasaki. *J. Radiat. Res.* **19**, 126–140 (1978).
28. M. C. Yoshida, T. Ikeuchi and M. Sasaki, Differential staining of parental chromosomes in interspecific cell hybrids with a combined quinacrine and 33258 Hoechst technique. *Proc. Jpn. Acad.* **51**, 185–187 (1975).
29. S. Miltenyi, W. Müller, W. Weichel and A. Radbruch, High gradient magnetic cell separation with MACS. *Cytometry* **11**, 231–238 (1990).
30. D. T. Fearon, P. Manders and S. D. Wagner, Arrested differentiation, the self-renewing memory lymphocyte, and vaccination. *Science* **293**, 248–250 (2001).
31. N. Nakamura, M. Nakano, Y. Kodama, K. Ohtaki, J. Cologne and A. A. Awa, Prediction of clonal chromosome aberration frequency in human blood lymphocytes. *Radiat. Res.* **161**, 282–289 (2004).
32. M. Nakano, Y. Kodama, K. Ohtaki, M. Itoh, R. Delongchamp, A. A. Awa and N. Nakamura, Detection of stable chromosome aberrations by FISH in A-bomb survivors: comparison with previous solid Giemsa staining data on the same 230 individuals. *Int. J. Radiat. Biol.* **77**, 971–977 (2001).
33. M. N. Cornforth, K. M. Greulich-Bode, B. D. Loucas, J. Arsuaga, M. Vazquez, R. K. Sachs, M. Bruckner, M. Molls, P. Hahnfeldt and D. J. Brenner, Chromosomes are predominantly located randomly with respect to each other in interphase human cells. *J. Cell Biol.* **159**, 237–244 (2002).
34. A. Wack, A. Cossarizza, S. Heltai, D. Barbieri, S. D'Addato, C. Franceschi, P. Dellabona and G. Casorati, Age-related modifications of the human alpha/beta T cell repertoire due to different clonal expansions in the $CD4^+$ and $CD8^+$ subsets. *Int. Immunol.* **10**, 1281–1288 (1998).
35. D. N. Posnett, R. Sinha, S. Kabak and C. Russo, Clonal populations of T cells in normal elderly humans: The T cell equivalent to "benign monoclonal gammapathy". *J. Exp. Med.* **179**, 609–618 (1994).
36. R. Schwab, P. Szabo, J. S. Manavalan, M. E. Weksler, D. N. Posnett, C. Pannetier, P. Kourilsky and J. Even, Expanded $CD4^+$ and $CD8^+$ T cell clones in elderly humans. *J. Immunol.* **158**, 4493–4499 (1997).
37. J. K. Morley, F. M. Batliwalla, R. Hingorani and P. K. Gregersen, Oligoclonal $CD8^+$ T cells are preferentially expanded in the $CD57^+$ subset. *J. Immunol.* **154**, 6182–6190 (1995).
38. P. Dellabona, G. Casorati, B. Friedli, L. Angman, F. Sallusto, A. Tunnacliffe, E. Roosneek and A. Lanzavecchia, *In vivo* persistence of expanded clones specific for bacterial antigens within the human T cell receptor alpha/beta $CD4^-$–8^- subset. *J. Exp. Med.* **177**, 1763–1771 (1993).
39. Y. Kusunoki, Y. Hirai, S. Kyoizumi and M. Akiyama, Evidence for *in vivo* clonal proliferation of unique population of blood $CD4^-$/$CD8^-$ T cells bearing T-cell receptor alpha and beta chains in two normal men. *Blood* **79**, 2965–2972 (1992).
40. Y. Kusunoki, Y. Hirai, T. Hayashi, S. Kyoizumi, K. Takahashi, Y. Morishita, Y. Kodama and M. Akiyama, Frequent occurrence of *in vivo* clonal expansion of $CD4^-$ $CD8^-$ T cells bearing T cell receptor alpha beta chains in adult humans. *Eur. J. Immunol.* **23**, 2735–2739 (1993).
41. E. Marshall, Gene therapy. Second child in French trial is found to have leukemia. *Science* **299**, 320 (2003).

INFECTION AND IMMUNITY, Feb. 2004, p. 871–879 Vol. 72, No. 2
0019-9567/04/$08.00+0 DOI: 10.1128/IAI.72.2.871–879.2004

Caspase-2 and Caspase-7 Are Involved in Cytolethal Distending Toxin-Induced Apoptosis in Jurkat and MOLT-4 T-Cell Lines

Masaru Ohara,[1] Tomonori Hayashi,[2] Yoichiro Kusunoki,[2] Mutsumi Miyauchi,[3] Takashi Takata,[3] and Motoyuki Sugai[1]*

Departments of Bacteriology[1] and Oral Maxillofacial Pathology,[3] Hiroshima University Graduate School of Biomedical Sciences, Hiroshima 734-8553, and Department of Radiobiology and Molecular Epidemiology, Radiation Effects Research Foundation, Hiroshima 732-0815,[2] Japan

Received 20 May 2003/Returned for modification 12 August 2003/Accepted 22 October 2003

Cytolethal distending toxin (CDT) from *Actinobacillus actinomycetemcomitans* is a G_2/M cell-cycle-specific growth-inhibitory toxin that leads to target cell distension followed by cell death. To determine the mechanisms by which *A. actinomycetemcomitans* CDT acts as an immunosuppressive factor, we examined the effects of highly purified CDT holotoxin on human T lymphocytes. Purified CDT was cytolethal toward normal peripheral T lymphocytes that were activated by in vitro stimulation with phytohemagglutinin. In addition, purified CDT showed cytolethal activity against Jurkat and MOLT-4 cells, which are known to be sensitive and resistant, respectively, to Fas-mediated apoptosis. Death in these cell lines was accompanied by the biochemical features of apoptosis, including membrane conformational changes, intranucleosomal DNA cleavage, and an increase in caspase activity in the cells. Pretreatment of Jurkat cells with the general caspase inhibitor z-VAD-fmk mostly suppressed CDT-induced apoptosis. Furthermore, specific inhibitors of caspase-2 and -7 showed significant inhibitory effects on CDT-induced apoptosis in Jurkat cells, and these inhibitory effects were fully associated with reduced activity of caspase-2 or -7 in the CDT-treated Jurkat cells. These results strongly suggest that CDT possesses the ability to induce human T-cell apoptosis through activation of caspase-2 and -7.

Bacterial infections in mammals evoke a series of immune reactions to bacterial antigens in the infected host, but immune responses are occasionally suppressed or shut down by some bacterial products, such as toxins. Suppression or inactivation of the host immune response is considered to be a bacterial strategy to evade host immune mechanisms. *Actinobacillus actinomycetemcomitans* is a gram-negative rod-shaped pathogen implicated in the pathogenesis of juvenile and adult periodontitis (38). Previous studies demonstrated that *A. actinomycetemcomitans* produces a factor(s) that is immunosuppressive for human T and B cells (25). It was recently established that *A. actinomycetemcomitans* produces a new member of the cytolethal distending toxin (CDT) family which was previously unrecognized as a virulence factor of *A. actinomycetemcomitans* (40). CDT belongs to the family of toxins with cell-cycle-specific inhibitory activities which block the progression of cells from G_2 to M phase (28). CDT-poisoned cells undergo cell distension and nucleus swelling and eventually die. CDT was found to form a complex of three subunits, CDTA, -B, and -C (9, 14, 21, 24, 31, 40), and the subunits were determined to be tandemly encoded by the *cdtA*, *cdtB*, and *cdtC* genes at the chromosomal *cdt* loci. *A. actinomycetemcomitans* CDTA, -B, and -C are translated as approximately 25-, 32-, and 21-kDa proteins, respectively, and are secreted into the periplasm (40). After cleavage of their 15- to 21-amino-acid signal sequences at the N terminus, they become 23-, 29-, and 19-kDa proteins, respectively (31, 36, 40). CDTA goes through another processing step to become an 18- to 19-kDa form, designated CDTA′, and forms a complex with CDTB and CDTC to become a holotoxin (40).

In 1999, Shenker et al. purified the immunosuppressive factor of *A. actinomycetemcomitans* that could affect human T cells and demonstrated that the factor was one of the subunit proteins of CDT, CDTB (34, 36). Their group also demonstrated that a crude CDT preparation of *A. actinomycetemcomitans* induced cell cycle arrest at the G_2 phase in human peripheral blood cells (37). Furthermore, the CDT preparation was shown to induce apoptotic cell death in peripheral blood lymphocytes along with activation of caspase-3, -8, and -9 (35). Despite those findings, whether these caspases are really involved in CDT-induced apoptosis remains virtually unknown.

For this study, we studied the immunosuppressive effect of highly purified *A. actinomycetemcomitans* CDT on normal human T lymphocytes and made an in-depth characterization of the cytolethal effect by using the T-cell leukemia cell lines Jurkat and MOLT-4, which are sensitive and resistant, respectively, to Fas-mediated apoptosis. We herein demonstrate that CDT induces apoptosis in these cells and that caspase-2 and -7 play important roles in the signaling pathway of CDT-induced cell death, which is distinct from Fas-mediated apoptosis.

MATERIALS AND METHODS

Purification of *A. actinomycetemcomitans* CDT. CDT holotoxin was prepared by using the pQE 60 (C-terminal histidine tag) protein expression system in M15 *Escherichia coli* (Qiagen, Tokyo, Japan). Briefly, for construction of pQE*cdtABC*, the *A. actinomycetemcomitans cdtABC* gene was isolated from *A. actinomycetemcomitans* genomic DNA by PCR amplification with specific primers that contained several restriction enzyme sites for subcloning into vectors, as follows: QIA-U, 5′-AGGTA*CCATGG*AAAAGTTT-3′, which corresponds to the *cdtA* starting site with an *Nco*I restriction enzyme site; QIC-L, 5′-AA*AGATCT*GCT ACCCTGA-3′, which corresponds to the end of the *cdtC* gene, with the stop

* Corresponding author. Mailing address: Department of Bacteriology, Hiroshima University Graduate School of Biomedical Sciences, Kasumi 1-2-3, Minami-ku, Hiroshima, Hiroshima 734-8553, Japan. Phone: (81) 82 257 5635. Fax: (81) 82 257 5639. E-mail: sugai@hiroshima-u.ac.jp.

codon replaced with a *Bgl*II site (restriction sites are shown in italics). The amplified *cdtABC* gene was ligated into pQE60 in frame at the *Nco*I and *Bgl*II sites, so that the C-terminal CDTC was tagged with six histidine residues. The expression of the *cdtABC* gene was induced by adding isopropyl-β-D-1-thiogalactopyranoside (final concentration of 1 mM; Sigma) at an optical density at 660 nm of 0.5 to 0.7. After induction for 4 h, the culture supernatant was harvested by centrifugation at 5,000 × *g* for 5 min, and crude proteins were precipitated with ammonium sulfate (final concentration, 80%) by gentle stirring for at least 4 h. The precipitates were recovered by centrifugation at 15,000 × *g* for 20 min, dissolved in phosphate-buffered saline (PBS) (137 mM NaCl, 2.7 mM KCl, 8.1 mM Na_2HPO_4, 1.5 mM KH_2PO_4), and dialyzed overnight against PBS. Ni-chelated agarose beads were added into the dialyzed solution and gently shaken for at least 1 h, followed by column chromatography. The column was washed with washing buffer (50 mM NaH_2PO_4 [pH 8.0], 300 mM NaCl, 20 mM imidazole) and eluted with elution buffer (50 mM NaH_2PO_4 [pH 8.0], 300 mM NaCl, 250 mM imidazole). The eluted CDT holotoxin was dialyzed against PBS and concentrated with Centricon 10 concentrators (Millipore, Bedford, Mass.).

Preparation of cells and culture conditions. Peripheral blood mononuclear cells were obtained from healthy volunteers with their informed consent. Twenty to forty milliliters of heparinized venous blood was diluted with an equal volume of PBS with 1% heparin and layered over Ficoll-Hypaque lymphocyte separation medium (ICN Biomedical Inc., Aurora, Ohio). Density gradient centrifugation was performed at 400 × *g* for 30 min, and mononuclear cells were harvested from the plasma-lymphocyte separation medium interface. Collected cells were washed twice with Earle's balanced salt solution (Nissui, Tokyo, Japan) containing 2.5% fetal calf serum (FCS) (Intergen Co., Purchase, N.Y.). The number of recovered cells was counted and diluted to 10^6 cells/ml in RPMI 1640 containing 10% FCS, 100 U of penicillin G/ml, and 100 μg of streptomycin/ml. The isolated lymphocytes were incubated with CDT (100 ng/ml) and cultured at 37°C in 5% CO_2, with or without stimulation on day 1 by phytohemagglutinin (PHA) (Difco Lab., Detroit, MI) diluted 1:1,600, and the cell population was monitored for 96 h. A thymic T-cell leukemia cell line, MOLT-4, and a peripheral T-cell leukemia cell line, Jurkat, were maintained in RPMI 1640 containing 10% FCS and 25 μg of kanamycin/ml at 37°C in 5% CO_2. The cells (10^6 cells/ml) were left untreated or were treated with CDT (100 ng/ml) and cultured under similar conditions. In some experiments, Jurkat cells were similarly treated with 100 ng of anti-CD95 (anti-Fas) monoclonal antibody (Ab) CH11 (BD PharMingen, San Diego, Calif.) per ml.

Flow cytometry. Conformational changes of the membrane by phosphatidylserine translocation and membrane hole formation were observed by counting the percentages of cells that were stained with fluorescein isothiocyanate (FITC)-labeled annexin V and propidium iodide (PI) in a FACScan flow cytometer (BD Biosciences, San Jose, Calif.). Briefly, CDT-treated cells (5 × 10^5 to 10 × 10^5) were collected by centrifugation at 350 × *g* for 2 min and were washed three times with 500 μl of PBS with 1% FCS. The washed cells were resuspended in 180 μl of PBS with 1% FCS, and 0.5 μl of FITC-labeled annexin V and 1 μl of PI, from the MEBCYTO apoptosis kit (MBL, Nagoya, Japan) were added to the cell suspension. After the reaction for 5 min at room temperature, 10,000 cells were analyzed in the FACScan instrument. The data obtained were processed by quadrant population analysis, using CellQuest software (BD Biosciences). The living cell population was determined by counting cells that were negative for both annexin V and PI (distributed in the lower left of the quadrant).

Caspase assay. CDT-treated cells were harvested and washed with PBS. PBS-washed cells were lysed with lysis buffer (10 mM Tris-Cl [pH 7.4], 25 mM NaCl, 0.25% Triton X-100, 1 mM EDTA) and centrifuged at 15,000 × *g* for 10 min. The supernatant was diluted with the lysis buffer and the protein concentration was adjusted to 1 mg/ml. Ten micrograms of total protein was incubated in 200 μl of caspase buffer (50 mM Tris-Cl [pH 7.2], 100 mM NaCl, 1 mM EDTA, 10% sucrose, 0.1% CHAPS, and 5 mM dithiothreitol) with a 50 μM concentration (each) of various fluorogenic substrate peptides. The peptides include Ac-DEVD-7-amino-4-methyl cumarine (AMC) for caspase-3, -7, and -8, Ac-DQTD-AMC for caspase-7 and -3, Ac-IETD-AMC for caspase-8, -6, and granzyme, Ac-LEHD-AMC for caspase-9, and Ac-VDVAD-AMC for caspase-2 (Peptide Institute Inc., Osaka, Japan).

The reaction mixture was incubated at 37°C for 60 min, and the release of 7-amino-4-methylcumarin was measured by use of a spectrophotometer (Shimazu RF-540), with excitation at 380 nm and emission at 460 nm. One unit (U) was defined as 5.2 pmol of substrate cleaved per min per mg of protein.

Various caspase inhibitors were used at a concentration of 100 μM. They were Ac-VAD-fmk as a general caspase inhibitor, Ac-WEHD-CHO for caspase-1, Ac-DEVD-CHO for caspase-3, -7, and -8, Ac-DMQD-CHO for caspase-3, Ac-LEHD-CHO for caspase-9, Ac-IETD-CHO for caspase-8 and -6, Ac-DQTD-CHO for caspase-7 and -3, and Ac-VDVAD-CHO for caspase-2 (Peptide Institute Inc.).

Electron microscopy. Cells were fixed with 2.5% glutaraldehyde for 2 h and rinsed in 0.1 M cacodylate buffer (pH 7.4) for 12 h. After postfixation with 1% osmium tetroxide for 30 min, cells were stained with 2% uranyl acetate for 30 min and dehydrated in graded alcohol, which was then replaced by propylene oxide. After these steps, the cell suspension was spun down at 8,000 × *g* for 5 min and the supernatant was discarded. The cell pellets were embedded in epoxy resin. Thin sections were stained in 2% uranyl acetate and lead citrate and were observed in a Hitachi H500 electron microscope.

Preparation of cytosolic and mitochondrial fractions. CDT-treated cells were washed twice with PBS and resuspended in isotonic buffer (10 mM HEPES [pH 7.3], 0.3 M mannitol, 0.1% bovine serum albumin). Digitonin was added to the cell suspension at a concentration of 0.1 mM, and the cells were incubated for 5 min on ice. After the samples were centrifuged at 8,500 × *g* for 5 min at 4°C, the supernatant was used as the cytosolic fraction. The pellet was resuspended in sonication buffer (50 mM Tris-HCl [pH 7.4], 150 mM NaCl, 2 mM EDTA, 1 mM phenylmethylsulfonyl fluoride, 0.5% Tween 20). The samples were sonicated with an ultrasonic disrupter (UD200 TOMY) for 20 s at output level 4. After centrifugation at 10,000 × *g* for 5 min at 4°C, the supernatant was collected and used as the mitochondrial fractions.

Antibodies. Antibodies against CDTA, -B, and -C that were previously obtained were used under conditions that were described elsewhere (40). Anti-cytochrome *c* Ab (BD PharMingen) was used according to the instructions provided by the supplier.

RESULTS

Cytolethal effects of highly purified CDT on human peripheral lymphocytes. *A. actinomycetemcomitans* CDT was purified from the culture supernatant of *E. coli* carrying the *A. actinomycetemcomitans cdtABC* genes. The secreted CDT complex was purified through a Ni chelation column, using the affinity of six histidine (His) residues tagged to the C terminus of CDTC (Fig. 1A). Sodium dodecyl sulfate-polyacrylamide gel electrophoresis and immunoblotting detected CDTA′, CDTB, and CDTC tagged with six histidine residues in the medium fraction, and premature CDTA was also found in a small amount, suggesting that most of the CDT complex consisted of CDTA′, CDTB, and CDTC. Cell distension and the G_2/M blocking activity of purified CDT were confirmed in HeLa cells, and the purified CDT complex was used for experiments.

To address whether CDT can induce cell death of human peripheral lymphocytes, we added purified CDT to peripheral blood mononuclear cell cultures in the presence or absence of PHA stimulation. Flow cytometry analysis with FITC-annexin V and PI revealed that treatment of normal lymphocytes with a combination of CDT and PHA increased the percentage of dead cells (the sum of annexin V^+ PI^+ and annexin V^+ PI^- fractions) (Fig. 1B). It should be noted that CDT did not kill lymphocytes very much unless they were activated with PHA. This is in good agreement with the previously suggested activity of CDT, which is cell-cycle-dependent cytotoxicity against HeLa cells (1), and also suggests that CDT can act as an immunosuppressive toxin by killing activated lymphocytes.

CDT induced apoptosis in Jurkat and MOLT-4 cells. In order to obtain further insights into the cytolethal effect of CDT in T lymphocytes, we used two cell lines, Jurkat and MOLT-4, and monitored population changes in four panels (upper left, upper right, lower left, and lower right [UL, UR, LL, and LR, respectively]) after CDT treatment (Fig. 2). For both cell lines, CDT treatment increased the percentage of dead cells (Fig. 2A). Flow cytometry analysis revealed that the percentage of annexin V^+ PI^- Jurkat cells (distributed in the

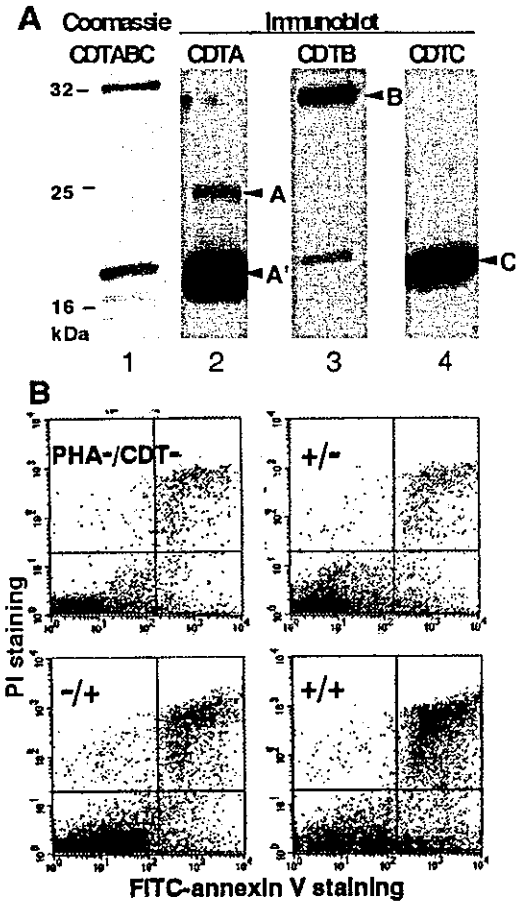

FIG. 1. Cytolethal effect of *A. actinomycetemcomitans* CDT on human peripheral lymphocytes. (A) Purified CDTABC complex in the medium fraction from *E. coli* M15 carrying *A. actinomycetemcomitans cdtABC*. Lane 1, Coomassie staining of CDTABC complex; lanes 2 to 4, immunoblots for the detection of each subunit by use of antiserum against CDTA, CDTB, and CDTC, respectively. Arrowheads: A, CDTA (premature form); A′, CDTA′ (mature form of CDTA); B, mature CDTB; C, mature CDTC tagged with six histidine residues. (B) Flow cytometry analysis. Lymphocytes were stained with FITC-labeled annexin V and PI and analyzed in a FACScan flow cytometer. Lymphocytes prepared from peripheral blood obtained from healthy human volunteers were treated with several combinations of PHA (1:1,600) and CDT (100 ng/ml). A representative result of the quadrant analysis of annexin V- and PI-stained lymphocytes on day 2 is shown.

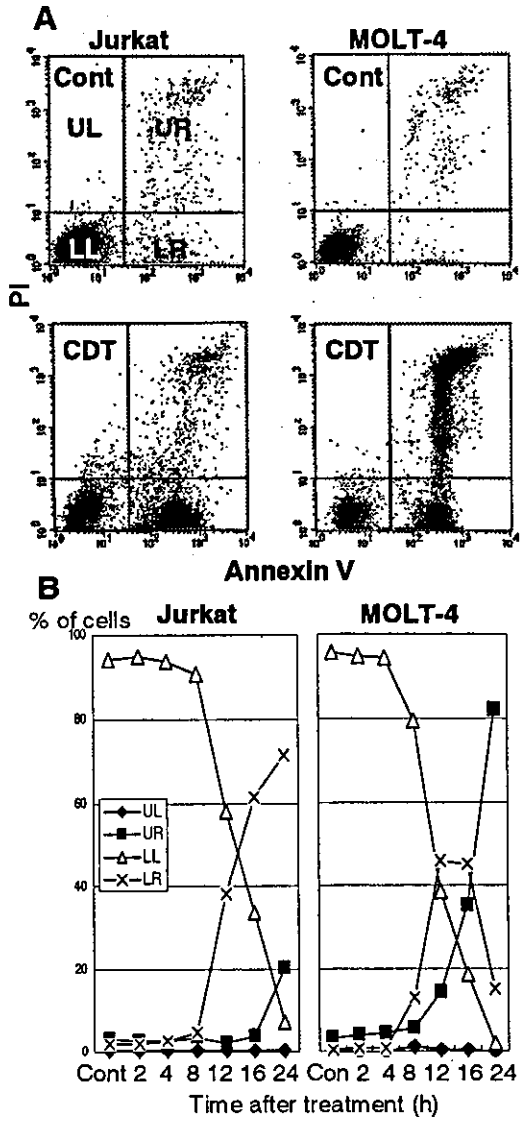

FIG. 2. Cytolethal kinetics on CDT-treated cell lines. T-cell leukemia cell lines Jurkat and MOLT-4 were treated with CDT (100 ng/ml) for various times. Cells stained with FITC-labeled annexin V and PI were analyzed by flow cytometry. (A) Representative results for cells with or without treatment of CDT at 16 h. Cont, control. (B) Kinetics of cell death measured at indicated times after CDT treatment. The percentages of cell populations in the UL quadrant (annexin V^- PI^+, ♦), the UR quadrant (annexin V^+ PI^+, ■), the LL quadrant (annexin V^- PI^-, △), and the LR quadrant (annexin V^+ PI^-, ×) are indicated.

LR panel) started to increase 8 h after CDT treatment and continued to increase until 24 h after treatment (Fig. 2B). MOLT-4 showed a somewhat different pattern from that of Jurkat. The percentage of annexin V^+ PI^- MOLT-4 cells (LR) started to increase 4 h after CDT treatment and reached a plateau 12 to 16 h after the treatment (Fig. 2B). After that, the annexin V^+ PI^- population (LR) decreased after 16 h. Concomitantly with the increase and decrease of the annexin V^+ PI^- population (LR), the annexin V^+ PI^+ population (UR) started to increase after 8 h and kept increasing until 24 h. In both cell lines, the increase of the annexin V^+ PI^- cell population (LR) in the early stage after treatment strongly suggested that CDT poisoning was able to induce apoptosis in cells that are sensitive to Fas-mediated apoptosis as well as in those that are resistant to Fas-mediated apoptosis. We further investigated the apoptotic characteristics of CDT-poisoned cells, including chromosomal DNA fragmentation and chromatin condensation. As shown in Fig. 3A, electrophoretic analysis of the chromosomal DNA of Jurkat cells showed a typical DNA ladder formation after 16 h of treatment with CDT, which is similar to those observed after treatment with anti-Fas Ab or irradiation. Electron microscopic observation of CDT-poisoned Jurkat cells revealed chromatin condensation, which is associated with cells undergoing apoptosis (Fig. 3B). Similar apoptotic characteristics were also apparent for CDT-treated MOLT-4 cells (data not shown). There was no necrotic change,

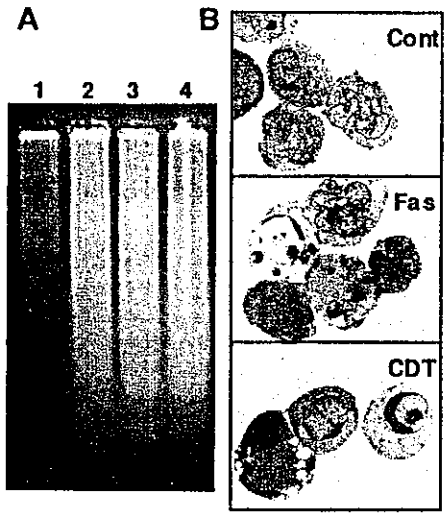

FIG. 3. Apoptotic DNA fragmentation and morphological change in CDT-treated lymphocytes. (A) DNA ladder formation in CDT-treated cells. Jurkat cells were treated with anti-Fas Ab (100 ng/ml) (lane 2), X-ray irradiation (10 Gy) (lane 3), or CDT (100 ng/ml) (lane 4) for 16 h, and chromosomal DNAs were prepared. The extracted DNAs were separated by agarose gel electrophoresis and visualized by staining with ethidium bromide. Lane 1, DNA from untreated Jurkat cells. (B) Ultrastructure of CDT- or anti-Fas Ab-treated lymphocytes. Jurkat cells were treated with CDT (100 ng/ml) for 16 h and subjected to electron microscopic observation as described in Materials and Methods. Cont, control.

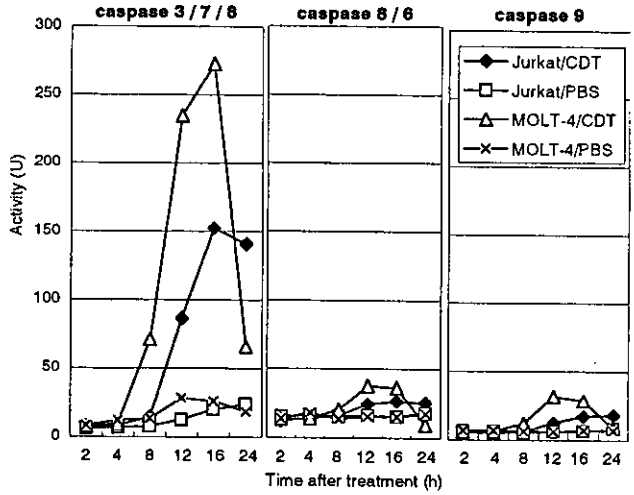

FIG. 4. Caspase activity in CDT-treated lymphocytes. The total protein (10 μg) was extracted from CDT-treated Jurkat or MOLT-4 cells at the indicated times. Caspase activity was measured by incubation of the extract with a fluorogenic substrate for caspase-3, -7, and -8 (left), caspase-8 and -6 (middle), or caspase-9 (right). After incubation, the released 7-amino-4-methylcumarine was measured in spectrophotometer, with excitation at 380 nm and emission at 460 nm. ♦, CDT-treated Jurkat cells; □, PBS-treated Jurkat cells (control); △, CDT-treated MOLT-4; ×, PBS-treated MOLT-4 (control). The experiments were repeated at least three times, and similar results were obtained. Representative results are shown.

such as swelling of the cell body and mitochondria or collapse of the plasma and nuclear membranes, in these cell lines.

Intracellular caspase activities. Apoptosis generally involves the activation of cysteine proteases, or caspases. The activity of sets of the major caspases, caspase-3, -7, and -8, caspase-8 and -6, and caspase-9, in Jurkat and MOLT-4 cells was monitored after CDT treatment. In Jurkat cells, the activity of caspase-3, -7, and -8 started to increase 8 h after treatment of the cells with CDT and significantly increased until 16 to 24 h (Fig. 4). On the other hand, the activity of the caspase-8 and -6 set and caspase-9 slightly increased upon treatment with CDT. Interestingly, caspase activity in MOLT-4 cells started to increase earlier and occurred at a higher level than in Jurkat cells between 4 and 16 h after treatment. After 12 to 16 h, caspase activity in MOLT-4 cells went down in parallel with the appearance of the annexin V^+ PI^- cell population (Fig. 4, Fig. 2B).

Cells retained the phenotype of living cells (annexinV^- PI^-) when the cells were pretreated with a general caspase inhibitor, z-VAD-fmk (100 μM), indicating that z-VAD-fmk is able to nearly completely inhibit CDT-induced apoptosis (Fig. 5A and B). It also turned out that the CDT-induced elevation of caspase activity could be blocked by z-VAD-fmk (Fig. 5C). These results indicated that CDT-induced apoptotic cell death in Jurkat and MOLT-4 cells was mostly dependent on the activation of a caspase(s) until at least 24 h after treatment.

Signaling pathway of caspases. Caspases can be classified into two categories as follows: initiator caspases, including caspase-2, -8, and -9, which are present upstream of the signaling pathway of apoptosis, and effector caspases, which play roles in the cleavage of many regulatory proteins (3). In order to determine the signaling pathway of the caspase(s) in CDT-induced apoptosis, we added a variety of caspase inhibitors and monitored their inhibitory effects on CDT cytotoxicity and apoptotic features in Jurkat cells by using flow cytometry with annexin V-PI double staining. For Fas-mediated apoptosis, caspase-8 was confirmed to be a critical initiator caspase for receptor-mediated apoptosis signaling in Jurkat cells, since the addition of Ac-IETD-CHO, an inhibitor of caspase-8 and -6, significantly inhibited the death of Jurkat cells by an anti-Fas Ab (Fig. 6A and C). On the other hand, inhibitors for caspase-3 (Ac-DMQD-CHO), caspase-8 and -6 (Ac-IETD-CHO), and caspase-9 (Ac-LEHD-CHO) failed to inhibit CDT-induced apoptosis of Jurkat cells (Fig. 6B and C), suggesting that CDT-induced apoptosis might use a different signaling pathway from that of Fas-mediated apoptosis. To determine which caspase(s) among those we tested is actually involved in CDT-induced apoptosis, we analyzed the effects of inhibitors of caspase-1 (Ac-WEHD-CHO), caspase-2 (Ac-VDVAD-CHO), and caspase-3, -7, and -8 (Ac-DEVD-CHO) on CDT-induced apoptosis. The inhibitor of caspase-1 (Ac-WEHD-CHO) had no inhibitory effect on CDT-induced apoptosis of Jurkat cells at concentrations up to 200 μM. On the other hand, CDT-induced apoptosis was dose dependently inhibited by the inhibitor of caspase-2 (VDVAD) or that of caspase-3, -7, and -8 (DEVD) (Fig. 7A and B). However, the combination of inhibitors of caspase-2 (VDVAD) and of caspase-3, -7, and -8 (DEVD) did not show any multiplier effect (Fig. 7C). Together with the fact that inhibitors of caspase-3 (Ac-DMQD-CHO) and caspase-8 and -6 (Ac-IETD-CHO) failed to prevent CDT-induced apoptosis (Fig. 6), our results strongly suggested

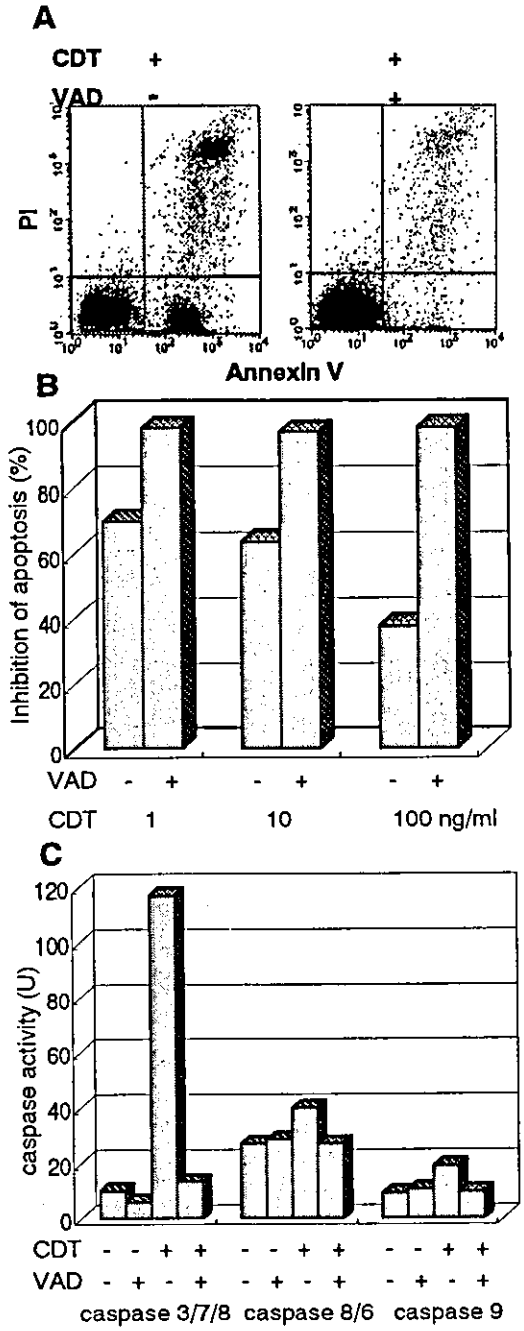

FIG. 5. Effect of general caspase inhibitor on CDT-induced apoptosis. (A) Jurkat cells were preincubated with z-VAD-fmk (100 μM) for 30 min and then were treated with CDT (1, 10, or 100 ng/ml) for 16 h. Cells were stained with FITC-annexin V and PI and analyzed by flow cytometry. The flow cytometry pattern represents CDT (100 ng/ml)-treated lymphocytes with (+) or without (−) z-VAD-fmk. Inhibition of apoptosis was calculated as the relative percentage of living cells, or the population in the LL quadrant (annexin V^- PI^- population). (B) z-VAD-fmk inhibits apoptosis in the cells treated with various concentrations of CDT. (C) Effect of z-VAD-fmk on caspase-3, -7, and -8, caspase-8 and -6, and caspase-9 activity induced by CDTB. Jurkat cells were preincubated with z-VAD-fmk (100 μM) for 30 min and then were treated with CDT (100 ng/ml). Caspase activity was measured as described in Materials and Methods.

that caspase-2 and -7 were mainly involved in the activation of this caspase-dependent apoptotic cascade. We therefore measured the activities of caspase-2 and -7 after CDT treatment for 16 h. To measure caspase-7 activity, we used Ac-DQTD-AMC (substrate for caspase-3 and -7) as a substrate because no caspase-7-specific substrate was available. As shown in Fig. 8A, CDT significantly induced the activation of caspase-2. CDT also induced caspase-3 and -7 activity, but the caspase-3-specific inhibitor Ac-DMQD-CHO did not inhibit the activity at all (Fig. 8A). This clearly indicated that the CDT treatment activated caspase-7. These data suggest that caspase-2 and caspase-7 are really involved in the pathway of CDT-induced apoptotic cell death. It is noteworthy that Ac-VDVAD-CHO (caspase-2 inhibitor) showed an inhibitory effect on caspase-3 and -7 activity. Similarly, Ac-DQTD-CHO (the caspase-3 and -7 inhibitor) clearly inhibited the effect on caspase-2. These results suggest that the caspase-2 and -7 pathways of CDT-induced apoptosis are tightly linked to each other, and they are quite consistent with the results of the experiment on the combination effect of inhibitors of caspase-2 and caspase-3, -7, and -8 (Fig. 7C). The incomplete inhibition of caspase-2 activity by Ac-VDVAD-CHO (caspase-2 inhibitor) implies that another molecule with proteolytic activity similar to that of caspase-2 may be involved in CDT-induced cell death.

To determine whether the mitochondrial pathway is really involved in CDT-induced apoptosis, we analyzed the release of cytochrome *c* from mitochondria in CDT-treated cells. As shown in Fig. 8B, the immunoblotting assay revealed that cytochrome *c* was detectable in the cytosol at 8 h, and more apparently so at 16 h, after CDT treatment of Jurkat cells. The appearance of cytochrome *c* accorded well with the time course of caspase activation, suggesting that the mitochondrial pathway is also involved in CDT-induced apoptosis.

DISCUSSION

In order to investigate CDT-induced apoptosis, we first attempted to establish a cell line model of it. Cytological and biological characterizations of CDT-treated Jurkat and MOLT-4 cells satisfied the apoptosis criteria, such as an increase in membrane conformational changes detected by an increase in the annexin V-positive cell population, intranucleosomal DNA fragmentation, chromatin condensation, and an increase in caspase activity (Fig. 1 to 4). It is noteworthy that the elevation of caspase activity in Jurkat and MOLT-4 cells showed some considerable differences in time course and in activation pattern: the culmination of induced caspase activity was higher in CDT-treated MOLT-4 cells than in similarly treated Jurkat cells. This may suggest that Jurkat and MOLT-4 cells took different apoptotic pathways after exposure to CDT. In this context, it should be noted that Jurkat, but not MOLT-4, cells are deficient in p53 (10). p53 is implicated in the G_2/M block in CDT-treated keratinocytes and fibroblasts (7). The phosphorylation of p53 and other phosphorylation signals could play some role in CDT-induced apoptosis, and the lack of p53 might alter the pathway of apoptosis of Jurkat cells from that of MOLT-4 cells.

We tried to obtain further insights into the understanding of the signaling pathway of CDT-induced apoptosis, especially regarding the caspase cascade(s). Caspases are members of the

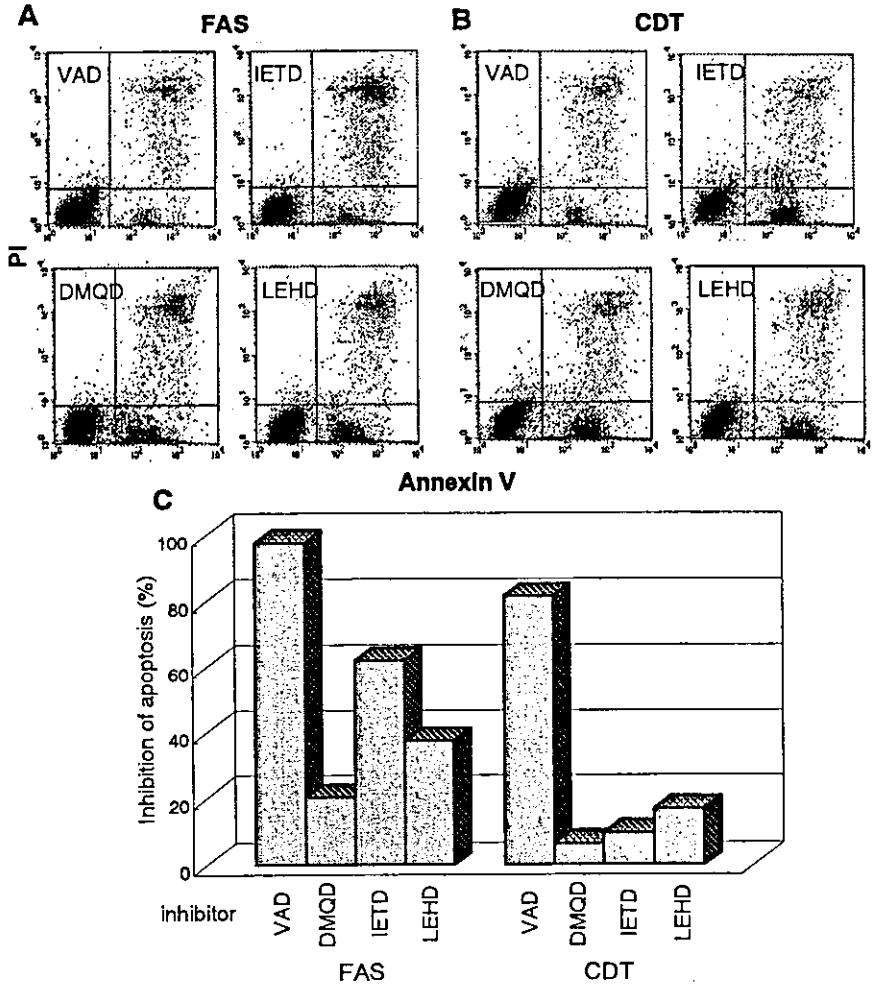

FIG. 6. Effect of various caspase inhibitors on CDT-induced apoptosis. Jurkat cells were preincubated with the indicated inhibitors (100 μM) for 30 min and then were treated with anti-Fas Ab (100 ng/ml) (A) or CDT (100 ng/ml) (B). After 16 h, cells were stained with FITC-annexin V and PI and analyzed by FACScan. The inhibitors used were VAD (general caspase inhibitor), DMQD (caspase-3 inhibitor), IETD (caspase-8 and -6 inhibitor), and LEHD (caspase-9 inhibitor). (A and B) Representative flow cytometry patterns. (C) Effect of caspase inhibitors on apoptosis induced by anti-Fas Ab (left) or CDT (right). Inhibition of apoptosis was defined as the relative percentage of normal living cells (annexin V^- PI^-).

aspartate-specific cysteine protease family which play a critical role in apoptosis (6, 39). They are composed of two major subfamilies, initiator caspases and effector caspases, based on the presence or absence of a large prodomain in the amino-terminal region (33). Initiator caspases generally act upstream of the proteolytic cascade, while effector caspases act downstream and are involved in the cleavage of specific cellular substrate proteins (41). Once processed, the substrates induce morphological changes characteristic of the apoptotic process (8, 11). The long prodomains of the initiator caspases trigger and/or facilitate the activation of proenzymes through interactions with adaptor molecules (13). Caspase-2, -8, -9, and -10 generally act as initiator caspases upstream of the cascade of effector caspases with small prodomains, such as caspase-3, -6, and -7 (26). Among the caspases, caspase-8, -9, and -10 play a fundamental role in transducing the specific apoptotic signal, and they cleave and activate effector procaspase-3, -6, and -7 (4). Effector caspases, in turn, cleave various proteins, leading to morphological and biochemical features characteristic of apoptosis. Recently, it has become clear that caspase-9 is involved in the apoptotic pathway that relys on mitochondrial dysfunction (15). Caspase-8 and -10 are involved in the apoptosis pathway mediated by death receptors (2).

Our results indicated that inhibitors of caspase-2 and -7 showed inhibitory effects on CDT-induced apoptosis. Several bacterial toxins are known to induce apoptosis through caspase-dependent pathways, although the exact molecular mechanism of the signaling cascade has not been well characterized. For instance, Shiga toxin and Shiga-like toxin have been demonstrated to activate caspase-2, -3, -6, -8, and -9 (5, 17, 18). It was suggested that these toxins use the caspase cascade involved in Fas-mediated apoptosis. Other toxins, such as *E. coli* heat-labile enterotoxin (32), *Clostridium difficile* toxin B (29), diphtheria toxin (19), and *Mannheimia haemolytica* leukotoxin (23), were shown to induce caspase-3. However, a detailed caspase cascade induced by bacterial toxins has not been well established. To our knowledge, this is the first report that a bacterial toxin preferentially utilizes caspase-2 and -7 in

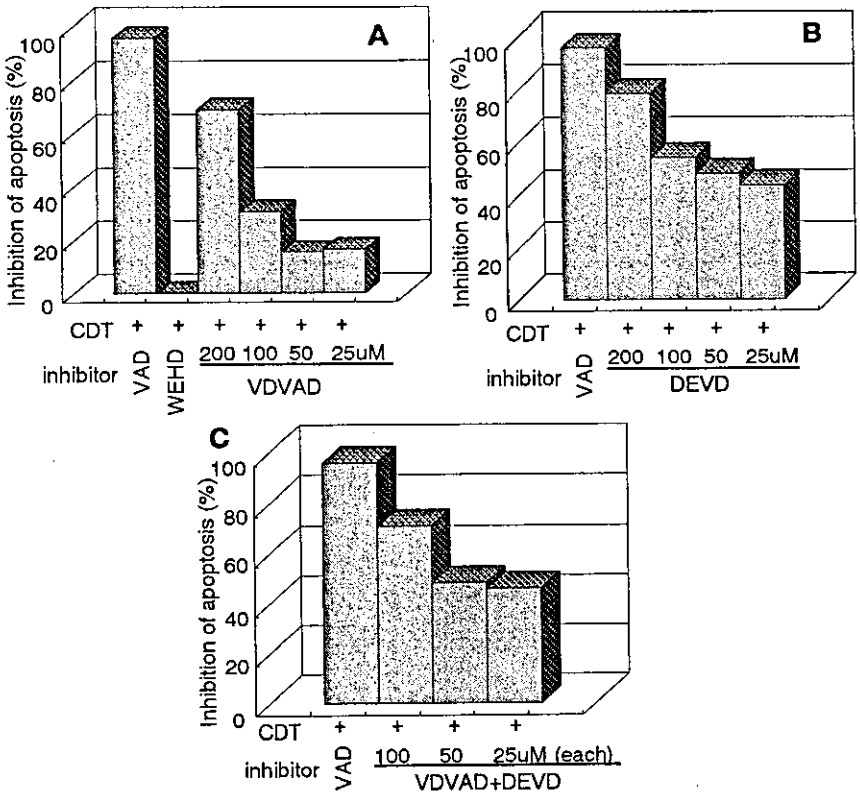

FIG. 7. Dose-dependent inhibitory effects of caspase inhibitors on CDT-induced apoptosis. Jurkat cells were preincubated with various concentrations of caspase inhibitors (25, 50, 100, and 200 μM) for 30 min and then were treated with CDT (100 ng/ml). The inhibitors used were WEHD (caspase-1 inhibitor), VDVAD (caspase-2 inhibitor), and DEVD (caspase-3, -7, and -8 inhibitor). After 16 h, cells were stained with FITC-annexin V and PI and analyzed by flow cytometry. Panels show the relative inhibition of CDT-induced apoptosis with VDVAD (A), DEVD (B), and VDVAD and DEVD (C). Inhibition of apoptosis was defined as the relative percentage of living cells (annexin V^- PI^-). VAD (general caspase inhibitor) and WEHD were used at concentrations of 100 and 200 μM, respectively.

the signaling pathway for apoptosis. In recent studies, caspase-2 was implicated in the release of cytochrome *c* from mitochondria in stress-induced apoptotic pathways (16, 22, 27, 30). One such stress-inducing agent is a topoisomerase II poison, etoposide, that induces double-stranded DNA breaks in cells. Robertson et al. (30) demonstrated that etoposide-induced DNA damage induces activation of caspase-2 and hence results in cytochrome *c* release from mitochondria and subsequent apoptosis. It is interesting that a possible mechanism by which CDT can induce cytopathic effects involves DNA strand breaks induced by its putative DNase activity (12, 20). Such CDT-induced DNA damage may trigger the mitochondrial cascade including caspase-2 and -7. A recent report has indicated the requirement of caspase-2 for the initiation of stress-induced apoptosis prior to mitochondrial permeabilization (22). In our case, CDT-induced DNA damage may directly activate caspase-2 and then induce the mitochondrial cascade, probably followed by caspase-7 activation. Caspase-7 is a late signal transducer and one of the members of the apoptosome complex which is activated by mitochondrial stress (3). Both caspase-2 and -7 are involved in stress-induced cascades, suggesting that CDT-induced apoptosis is related to the mitochondrial pathway. Our present results indicate that CDT can induce mitochondrial membrane permeabilization, resulting in the release of cytochrome *c*, and that this mitochondrial pathway is highly involved in CDT-induced apoptosis. This is quite in agreement with an experiment showing that Bcl-2 overexpression reduces apoptosis in a CDT-treated human B lymphoblastoid cell line, JY (35).

Fas ligation on the cell surface induces apoptosis through the receptor-mediated signaling pathway, which involves caspase-8 as an initiation signal (2). The fact that caspase-8 inhibitor blocked Fas-mediated apoptosis in Jurkat cells (Fig. 6) indicated that the Fas-dependent apoptotic pathway was active in this cell line. In contrast, no inhibitory effect of caspase-8 inhibitor on CDT-induced apoptosis was observed in Jurkat cells, suggesting that the cytotoxic effect of CDT does not require the activation of death receptors on the cell surface.

Since CDT is able to induce apoptosis of activated T cells, this toxin may play an important role in that the bacteria evade T-cell immune responses in the periodontal pocket. It is conceivable that CDT produced by this pathogen exacerbates local inflammation by inducing apoptotic cell death of T lymphocytes that are responsible for the clearance of bacteria from the periodontal pocket. Further studies on the effect of CDT on the caspase network should unveil the CDT-related signal transduction pathway in T-lymphocyte apoptosis that may lead to the suppression of immune responses to the pathogen.

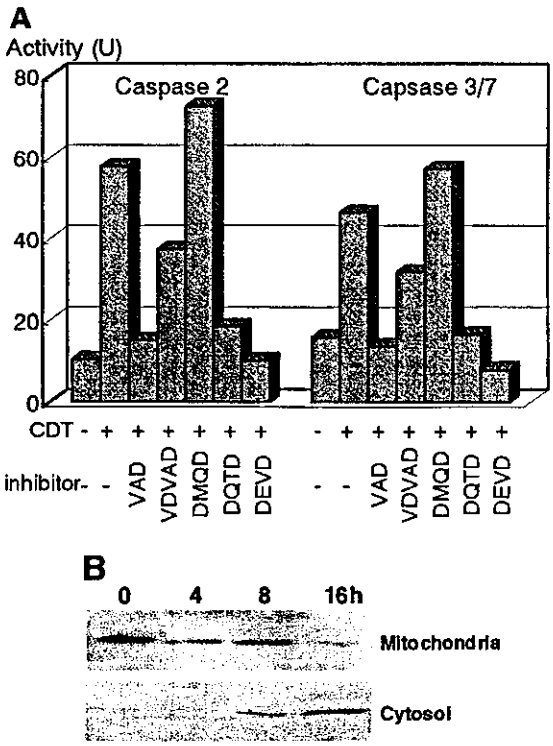

FIG. 8. Elevation of caspase-2 or -7 activity and cytochrome *c* release by CDT treatment. (A) Jurkat cells were preincubated with the indicated inhibitor (100 μM) for 30 min and then were treated with CDT (100 ng/ml) for 16 h. The inhibitors used were VAD (general caspase inhibitor), VDVAD (caspase-2 inhibitor), DMQD (caspase-3 inhibitor), DQTD (caspase-3 and -7 inhibitor), and DEVD (caspase-3, -7, and -8 inhibitor). Caspase activity was measured as described in Materials and Methods. (B) Cytosol and mitochondrial fractions were extracted from Jurkat cells that were treated with CDT (100 ng/ml) for 0, 4, 8, and 16 h and were subsequently immunoblotted with an anti-cytochrome *c* Ab followed by a horseradish peroxidase-conjugated secondary Ab. The bands of cytochrome *c* were visualized by ECL.

ACKNOWLEDGMENTS

We thank Kei Nakachi, Donald G. MacPhee, and Seishi Kyoizumi at the Department of Radiobiology and Molecular Epidemiology, Radiation Effects Research Foundation, for helpful suggestions. We thank the Research Facilities, Hiroshima University School of Dentistry and School of Medicine, for the use of facilities.

This study was supported in part by a Grant for Development of Highly Advanced Medical Technology (A) and by a Grant-in-Aid for Scientific Research (B) from the Ministry of Education, Science, Sports and Culture of Japan.

REFERENCES

1. **Alby, F., R. Mazars, J. De Rycke, E. Guillou, V. Baldin, J.-M. Darbon, and B. Ducommun.** 2001. Study of the cytolethal distending toxin (CDT)-activated cell cycle checkpoint. Involvement of the CHK2 kinase. FEBS Lett. **491**:261–265.
2. **Ashkenazi, A., and V. M. Dixit.** 1998. Death receptors: signaling and modulation. Science **281**:1305–1308.
3. **Bratton, S. B., M. Macfarlane, K. Cain, and G. M. Cohen.** 2000. Protein complexes activate distinct caspase cascades in death receptor and stress induced apoptosis. Exp. Cell Res. **256**:27–33.
4. **Budihardjo, I., H. Oliver, M. Lutter, X. Luo, and X. Wang.** 1999. Biochemical pathways of caspase activation during apoptosis. Annu. Rev. Cell Dev. Biol. **15**:269–290.
5. **Ching, J. C., N. L. Jones, P. J. Ceponis, M. A. Karmali, and P. M. Sherman.** 2002. *Escherichia coli* Shiga-like toxins induce apoptosis and cleavage of poly(ADP-ribose) polymerase via in vitro activation of caspases. Infect. Immun. **70**:4669–4677.
6. **Cohen, G. M.** 1997. Caspases: the executioners of apoptosis. Biochem. J. **326**:1–16.
7. **Cortes-Bratti, X., C. Karlsson, T. Lagergard, M. Thelestam, and T. Frisan.** 2001. The *Haemophilus ducreyi* cytolethal distending toxin induces cell cycle arrest and apoptosis via the DNA damage checkpoint pathways. J. Biol. Chem. **276**:5296–5302.
8. **Cryns, V., and J. Yuan.** 1998. Proteases to die for. Genes Dev. **12**:1551–1570.
9. **Deng, K., J. L. Latimer, D. A. Lewis, and E. J. Hansen.** 2001. Investigation of the interaction among the components of the cytolethal distending toxin of *Haemophilus ducreyi*. Biochem. Biophys. Res. Commun. **20**:609–615.
10. **Dreyfus, D. H., M. Nagasawa, C. A. Kelleher, and E. W. Gelfand.** 2000. Stable expression of Epstein-Barr virus BZLF-1-encoded ZEBRA protein activates p53-dependent transcription in human Jurkat T-lymphoblastoid cells. Blood **96**:625–634.
11. **Earnshaw, W. C., L. M. Martins, and S. H. Kaufmann.** 1999. Mammalian caspases: structure, activation, substrates, and functions during apoptosis. Annu. Rev. Biochem. **68**:383–424.
12. **Elwell, C. A., K. Chao, K. Patel, and L. A. Dreyfus.** 2001. *Escherichia coli* CdtB mediates cytolethal distending toxin cell cycle arrest. Infect. Immun. **69**:3418–3422.
13. **Fesik, S. W.** 2000. Insights into programmed cell death through structural biology. Cell **103**:273–282.
14. **Frisk, A., M. Labens, C. Johansson, H. Ahmed, L. Svensson, K. Ahlman, and T. Lagergard.** 2001. The role of different protein components from the *Haemophilus ducreyi* cytolethal distending toxin in the generation of cell toxicity. Microb. Pathog. **30**:313–324.
15. **Green, D. R.** 2000. Apoptotic pathways: paper wraps stone blunts scissors. Cell **102**:1–4.
16. **Guo, Y., S. M. Srinivasula, A. Druilhe, T. Fernandes-Alnemri, and E. S. Alnemri.** 2002. Caspase-2 induces apoptosis by releasing proapoptotic proteins from mitochondria. J. Biol. Chem. **277**:13430–13437.
17. **Kiyokawa, N., T. Mori, T. Taguchi, M. Saito, K. Mimori, T. Suzuki, T. Sekino, N. Sato, H. Nakajima, Y. U. Katagiri, T. Takeda, and J. Fujimoto.** 2001. Activation of the caspase cascade during Stx-1-induced apoptosis in Burkitt's lymphoma cells. J. Cell. Biochem. **81**:128–142.
18. **Kojio, S., H. Zhang, M. Ohmura, F. Gondaira, N. Kobayashi, and T. Yamamoto.** 2000. Caspase-3 activation and apoptosis induction coupled with the retrograde transport of Shiga toxin: inhibition by brefeldin A. FEMS Immunol. Med. Microbiol. **29**:275–281.
19. **Komatsu, N., T. Oda, and T. Muramatsu.** 1998. Involvement of both caspase-like proteases and serine proteases in apoptotic cell death induced by ricin, modeccin, diphtheria toxin, and pseudomonas toxin. J. Biochem. (Tokyo) **124**:1038–1044.
20. **Lara-Tejero, M., and J. E. Galan.** 2000. A bacterial toxin that controls cell cycle progression as a deoxyribonuclease I-like protein. Science **290**:354–357.
21. **Lara-Tejero, M., and J. E. Galan.** 2001. CdtA, CdtB, and CdtC form a tripartate complex that is required for cytolethal distending toxin activity. Infect. Immun. **69**:4358–4365.
22. **Lassus, P., X. Opitz-Araya, and Y. Lazebnik.** 2002. Requirement for caspase-2 in stress-induced apoptosis before mitochondrial permeabilization. Science **297**:1352–1354.
23. **Leite, F., S. O'Brien, M. J. Sylte, T. Page, D. Atapattu, and C. J. Czuprynski.** 2002. Inflammatory cytokines enhance the interaction of *Mannheimia haemolytica* leukotoxin with bovine peripheral blood neutrophils in vitro. Infect. Immun. **70**:4336–4343.
24. **Lewis, D. A., M. K. Stevens, J. L. Latimer, C. K. Ward, K. Deng, R. Blick, S. R. Lumbley, C. A. Ison, and E. J. Hansen.** 2001. Characterization of *Haemophilus ducreyi cdtA*, *cdtB*, and *cdtC* mutants in in vitro and in vivo systems. Infect. Immun. **69**:5626–5634.
25. **Mangan, D. F., N. S. Taichman, E. T. Lally, and S. M. Wahl.** 1991. Lethal effects of *Actinobacillus actinomycetemcomitans* leukotoxin on human T lymphocytes. Infect. Immun. **59**:3267–3272.
26. **Nicholson, D. W., and N. A. Thornberry.** 1997. Caspases: killer proteases. Trends Biochem. Sci. **22**:299–306.
27. **Paroni, G., C. Henderson, C. Schneider, and C. Brancolini.** 2002. Caspase-2 can trigger cytochrome *c* release and apoptosis from the nucleus. J. Biol. Chem. **277**:15147–15161.
28. **Pickett, C. L., and C. A. Whitehouse.** 1999. The cytolethal distending toxin family. Trends Microbiol. **7**:292–297.
29. **Qa'Dan, M., M. Ramsey, J. Daniel, L. M. Spyres, B. Safiejko-Mroczka, W. Ortiz-Leduc, and J. D. Ballard.** 2002. *Clostridium difficile* toxin B activates dual caspase-dependent and caspase-independent apoptosis in intoxicated cells. Cell. Microbiol. **4**:425–434.
30. **Robertson, J. D., M. Enoksson, M. Suomela, B. Zhivotovsky, and S. Orrenius.** 2002. Caspase-2 acts upstream of mitochondria to promote cytochrome *c* release during etoposide-induced apoptosis. J. Biol. Chem. **277**:29803–29809.
31. **Saiki, K., K. Konishi, T. Gomi, T. Nishihara, and M. Yoshikawa.** 2001. Reconstitution and purification of cytolethal distending toxin of *Actinobacillus actinomycetemcomitans*. Microbiol. Immunol. **45**:497–506.
32. **Salmond, R. J., R. S. Pitman, E. Jimi, M. Soriani, T. R. Hirst, S. Ghosh, M. Rincon, and N. A. Williams.** 2002. $CD8^+$ T cell apoptosis induced by *Esch-*

erichia coli heat-labile enterotoxin B subunit occurs via a novel pathway involving NF-kappaB-dependent caspase activation. Eur. J. Immunol. **32:** 1737–1747.

33. **Salvesen, G. S., and V. M. Dixit.** 1999. Caspase activation: the induced-proximity model. Proc. Natl. Acad. Sci. USA **96:**10964–10967.
34. **Shenker, B. J., R. H. Hoffmaster, T. L. Mckay, and D. R. Demuth.** 2000. Expression of the cytolethal distending toxin (Cdt) operon in *Actinobacillus actinomycetemcomitans*: evidence that the CdtB protein is responsible for G_2 arrest of the cell cycle in human T cells. J. Immunol. **165:**2612–2618.
35. **Shenker, B. J., R. H. Hoffmaster, A. Zekavat, N. Yamaguchi, E. T. Lally, and D. Demuth.** 2001. Induction of apoptosis in human T cells by *Actinobacillus actinomycetemcomitans* cytolethal distending toxin is a consequence of G_2 arrest of the cell cycle. J. Immunol. **167:**435–441.
36. **Shenker, B. J., T. McKay, S. Datar, M. Miller, R. Chowhan, and D. Demuth.** 1999. *Actinobacillus actinomycetemcomitans* immunosuppressive protein is a member of the family of cytolethal distending toxins capable of causing a G_2 arrest in human T cells. J. Immunol. **162:**4773–4780.
37. **Shenker, B. J., L. Vitale, and C. King.** 1995. Induction of human T cells that coexpress CD4 and CD8 by an immunomodulatory protein produced by *Actinobacillus actinomycetemcomitans.* Cell. Immunol. **164:**36–46.
38. **Slots, J., H. S. Reynolds, and R. J. Genco.** 1980. *Actinobacillus actinomycetemcomitans* in human periodontal disease: a cross-sectional microbiological investigation. Infect. Immun. **29:**1013–1020.
39. **Stennicke, H. R., and G. S. Salvesen.** 1997. Biochemical characteristics of caspases-3, -6, -7, and -8. J. Biol. Chem. **272:**25719–25723.
40. **Sugai, M., T. Kawamoto, S. Y. Peres, Y. Ueno, H. Komatsuzawa, T. Fujiwara, H. Kurihara, H. Suginaka, and E. Oswald.** 1998. The cell cycle-specific growth-inhibitory factor produced by *Actinobacillus actinomycetemcomitans* is a cytolethal distending toxin. Infect. Immun. **66:**5008–5019.
41. **Thornberry, N. A., and Y. Lazebnik.** 1998. Caspases: enemies within. Science **281:**1312–1316.

Editor: V. J. DiRita

Available online at www.sciencedirect.com
SCIENCE DIRECT®
Biochemical and Biophysical Research Communications 320 (2004) 656–663
BBRC
www.elsevier.com/locate/ybbrc

Interaction of ligand–receptor system between stromal-cell-derived factor-1 and CXC chemokine receptor 4 in human prostate cancer: a possible predictor of metastasis

Hideki Mochizuki,[a] Akio Matsubara,[b] Jun Teishima,[b] Kazuaki Mutaguchi,[b] Hiroaki Yasumoto,[b] Rajvir Dahiya,[c,*] Tsuguru Usui,[b] and Kenji Kamiya[a]

[a] *Division of Genome Biology, Department of Experimental Oncology, Research Institute for Radiation Biology and Medicine, Hiroshima University, Hiroshima, Japan*
[b] *Programs for Biochemical Research, Division of Frontier Medical School, Department of Urology, Graduate School of Biomedical Sciences, Hiroshima University, Hiroshima, Japan*
[c] *Department of Urology and Urology Research Center, University of California San Francisco and Veterans Affairs Medical Center, USA*

Received 24 May 2004

Abstract

Interaction of ligand–receptor systems between stromal-cell-derived factor-1 (SDF-1) and CXC chemokine receptor 4 (CXCR4) is closely involved in the organ specificity of cancer metastasis. We hypothesized that SDF-1–CXCR4 ligand–receptor system plays an important role in prostate cancer metastasis. To test this hypothesis, expression level of SDF-1 and CXCR4 was analyzed in prostate cancer (PC) cell lines (LNCaP, PC3, and DU145) and normal prostate epithelial cell line (PrEC). We also performed migration assay and MTT assay to investigate the chemotactic effect and growth-promoting effect of SDF-1 on DU145 and PC3 cells, respectively. Furthermore, we performed immunohistochemical analysis of CXCR4 expression in tissues from 35 cases of human prostate cancer. CXCR4 expression was detected in all three prostate cancer cell lines, but not in PrECs. SDF-1 significantly enhanced the migration of PC3 and DU145 cells in a dose-dependent manner, and anti-CXCR4 antibody inhibited this chemotactic effect. However, SDF-1 itself did not significantly stimulate the cell growth rate of prostate cancer cell lines. Positive CXCR4 protein was found in 20 out of 35 clinical PC samples (57.1%). Three patients with lung metastasis showed definitely positive CXCR4 immunostaining. Logistic regression analysis revealed that positive expression of CXCR4 protein was an independent and superior predictor for bone metastasis to Gleason sum ($P < 0.05$). Furthermore, among PC patients with PSA greater than 20 ng/mL, the positive rate of CXCR4 protein was significantly higher in patients with bone metastasis than in those with no bone metastasis ($P = 0.017$). These findings suggest that the interaction between SDF-1 and CXCR4 ligand–receptor system is involved in the process of PC metastasis by the activation of cancer cell migration. This is the first report to investigate the role of interaction of ligand–receptor systems between SDF-1 and CXCR4 in prostate cancer metastasis.

Keywords: CXCR4; SDF-1; Prostate cancer; Metastasis

In advanced prostate cancer, the sites most frequently affected by metastasis are the bones and regional lymph nodes [1,2]. Patients with these metastases not only have a poor prognosis but also suffer pain and lower limb edema. It is therefore extremely important to elucidate the molecular mechanisms underlying prostate cancer metastases to the bones and/or lymph nodes and to explore the avenues preventing such metastases. The molecular processes associated with metastases such as migration of cancer cells, their adhesion to specific organs, and cell proliferation within the microcirculation of these organs have been fully investigated [1,2]. In this regard, it is assumed that the target organ specificity of cancer metastasis is followed by the similar mechanism

* Corresponding author. Fax: 1-415-750-6639.
E-mail addresses: rdahiya@urol.ucsf.edu (R. Dahiya), musui@hiroshima-u.ac.jp (T. Usui).

0006-291X/$ - see front matter © 2004 Elsevier Inc. All rights reserved.
doi:10.1016/j.bbrc.2004.06.013

observed in the homing of hematopoietic stem cells (HSC) to bone marrow in the accepted model of hematopoiesis [3–5]. Bone marrow stromal cells produce a chemokine, stromal-cell-derived factor-1 (SDF-1), especially during the process of fetal hematopoiesis and after bone marrow transplantation. At the same time, HSC significantly expresses its receptor, CXC chemokine receptor 4 (CXCR4) [3–5]. SDF-1 is a member of the CXC subfamily of chemokines, and its chemotactic and growth-promoting effects are mediated by CXCR4. Consequently, SDF-1 acts as a powerful chemo-attractant for HSC, which in turn "homes in" on the bone marrow specifically and efficiently [3–5].

Based on this hematopoiesis model, recent publications have demonstrated that the SDF-1–CXCR4 ligand–receptor system is closely involved in the organ specificity of cancer metastasis. For instance, Muller et al. [6] have reported that (i) CXCR4 is highly expressed in human breast cancer cells and (ii) the highest SDF-1 expression is observed in those organs that are usually the primary destinations of breast cancer metastases. SDF-1 signaling through CXCR4 interaction appears to determine the directional migration of breast cancer cells through the basement membrane. Furthermore in vivo, the interaction between SDF-1 and CXCR4 significantly represses the metastatic potential of breast cancer cells to regional lymph node and lung. These findings indicate that the SDF-1–CXCR4 ligand–receptor system plays a critical role in determining the metastatic destination of cancer cells. Similar experimental results have also been reported in other types of cancer such as malignant melanoma, ovarian, pancreatic, and lung [7–13]. However, such studies are limited in prostate cancer.

To investigate whether SDF-1–CXCR4 ligand–receptor system is involved in the metastasis of human prostate cancer, we investigated the gene and protein expression of CXCR4 in the prostate cancer cell lines LNCaP, PC3, and DU145, in comparison with normal prostate epithelial cells. We also investigated the chemotactic activity and the growth-promoting effect of SDF-1 on DU145 and PC3 cells. Furthermore, we performed CXCR4 immunostaining in clinical samples (35 human prostate cancer tissues and nine non-malignant human prostate tissues), and evaluated the relationship between CXCR4 expression and clinicopathological findings with special reference to cancer metastasis.

Materials and methods

Prostate tissue samples. Thirty-five prostate cancer samples (32 prostatic biopsy samples, 2 radical prostatectomy samples, and one transurethrally resected sample) and nine non-malignant prostate samples (seven normal prostate obtained at total cystoprostatectomy and two BPH tissues from suprapubic prostatectomy) were obtained with informed consent at the Department of Urology, Hiroshima University School of Medicine, Hiroshima, Japan, between 1998 and 2001. All tissue samples were pathologically diagnosed and confirmed to contain the objective parts. A single pathologist classified each sample according to the Gleason grading system [14]. Staging examination for PC included digital rectal examination, transrectal ultrasound, urethrocystography, computed tomography, magnetic resonance imaging, and bone scanning. The clinicopathological stage of prostate cancer was categorized according to the 1997 International Union Against Cancer (UICC) TNM classification [15]. Serum prostate-specific antigen (PSA) levels were measured by Tandem R assay (Hybritech, San Diego, CA, USA).

Cell culture. Human prostate cancer cell lines of LNCaP, PC-3, and DU145 were purchased from the American Type Culture Collection (Drive Rockville, MD, USA) and maintained in OPTI-MEM I medium (Life Technologies, Gaithersburg, MD, USA) supplemented with 5% fetal bovine serum (FBS), 1 mM $CaCl_2$, and 100 μg/mL kanamycin (Life Technologies). LNCaP cells were originally isolated from lymph node in a patient with hormone-dependent prostate cancer involved in bone and lymph node metastases. PC3 and DU145 cells were isolated from the regions of vertebral and brain metastases, respectively, in hormone-independent prostate cancer patients. These cell lines were cultured at 37 °C in a humid atmosphere of 5% CO_2 and passaged at approximately 70% confluence. Human normal prostate epithelial cell line, prostate epithelial cell (PrEC), was obtained from Clonetics (San Diego, CA, USA). PrECs were grown in PrECG Bullet Kit medium according to the manufacturer's instructions and used without passage.

Total RNA extraction and reverse transcriptase PCR (RT-PCR). Total RNA was extracted from each human prostate cancer cell line and PrEC line by the acid guanidium–phenol–chloroform method using Isogen (Nippon Gene, Tokyo, Japan). Pelvic lymph nodes taken from a bladder cancer patient (T2N0M0) were homogenized and used as positive controls of SDF-1 and CXCR4 expression [6,16,17]. The RNA pellet obtained after isopropanol and ethanol precipitation was dried and re-suspended in 50 μL RNase-free water. RNA specimens were stored and frozen in aliquots at −80 °C until reverse-transcribed. The concentration of RNA was determined by spectrophotometer, and their integrity was checked by agarose gel electrophoresis.

One microgram of RNA was added to 0.5 μg oligodeoxythymidilic acid primer (TaKaRa, Shiga, Japan) and prepared to a final volume of 20 μL. The samples were placed at 55 °C for 5 min and then cooled on ice. The primer–RNA mixture was then combined with 0.25 U Avian myeloblastosis virus reverse transcriptase (TaKaRa, Shiga, Japan) and 0.5 U RNase inhibitor. Finally, the mixture was added to 1 mM dNTP, 50 mM Tris–HCl, 75 mM KCl, and 5 mM $MgCl_2$. The reverse transcriptase reaction was then carried out at 45 °C for 45 min. The cDNA was then incubated at 95 °C for 5 min to inactivate the reverse transcriptase. Samples were stored at −20 °C until used.

Primer sets of PCR for CXCR4 (GenBank Accession No. XM_051225), SDF-1 [10] and β-actin were designed and synthesized (Amersham–Pharmacia Biotech, Tokyo, Japan) as follows: CXCR4 (347 bp): forward 5′-AGC TGT TGG CTG AAA AGG TGG TCT ATG-3′, reverse 5′-GCG CTT CTG GTG GCC CTT GGA GTG TG-3′; SDF-1 (380 bp): forward 5′-CCG CGC TCT GCC TCA GCG ACG GGA AG-3′, reverse 5′-CCT GTT TAA AGC TTT CTC CAG GTA CT-3′; and β-actin (696 bp): forward 5′-CAC CAA CTG GGA CGA CAT GG-3′, reverse 5′-CCA GGG TAC ATG GTG GTG CC-3′. The cDNA samples (2 μL) were diluted into 20 μL solution containing 50 mM dNTP, 500 nM of each primer, 0.5 U of *Taq* polymerase, and PCR buffer provided by the manufacturer (TaKaRa). Suitable PCR cycles for CXCR4, SDF-1, and β-actin were determined to remain within the linear range of the reaction. Briefly, after predenaturing at 94 °C for 4 min, 35 cycles of amplification comprising denaturing at 94 °C for 30 min, annealing at 50 °C for 1 min and extension at 72 °C for 1 min were performed using a thermal cycler (RoboCycler GRADIENT 96, Stratagene, CA, USA). The PCR products were electrophoresed on 2.0% agarose gels.